

國立臺灣大學工學院材料科學與工程研究所

碩士論文

Department of materials science and engineering

College of Engineering

National Taiwan University

Master Thesis

不同氧鈦比之氧化鈦分析及其於太陽能電池之應用

Analysis of different O/Ti ratio titanium oxide and its application
in Organic Photovoltaics



邵騰緯

Teng-Wei Shao

指導教授：陳俊維 博士

Advisor: Chun-Wei Chen, Ph.D.

中華民國 101 年 6 月

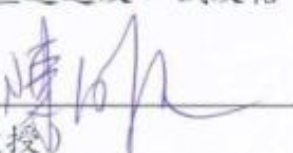
June, 2012

國立臺灣大學碩士學位論文 口試委員會審定書

論文中文題目： 不同氧鈦比之氧化鈦分析及其在有機太陽能電池上之應用

論文英文題目： Analysis of different O/Ti ratio titanium oxide and its application in organic photovoltaic

本論文係邵騰緯(R99527064)在國立臺灣大學材料科學與工程學系、所完成之碩士學位論文，於民國 101 年 6 月 26 日承下列考試委員審查通過及口試及格，特此證明

口試委員： 陳俊維 
(指導教授)

溫政彥 

吳季珍 

系主任、所長  (簽名)

Acknowledgements

想不到已是輪到我寫致謝的時候，也無怪乎有許多騷人詩客對光陰流逝有此多的感觸，我又何嘗不是呢！？

在研究所兩年中首要感謝的莫過於我的指導教授陳俊維老師，除了實驗上的方向，老師教會我更多的是做人處事的道理跟態度，這對未來出社會必會受用無窮的，真的要在這裡好好感謝老師。同時感謝口試委員溫政彥老師及吳季珍老師在口試時的指正及建議，使這本論文的内容更為完善。

研究所生涯中，首先感謝雲傑學長在實驗上給予我莫大的幫助，這兩年內若我有任何成長的地方必然有不少部份要歸功於學長。感謝紹先學長於論文上不遺餘力的指導使我能順利完成，感謝志誠學長在低潮時也能給予鼓勵及指導。感謝迪彥學長在實驗上的量測及提供我研究方向。感謝映樵學長，讓我對二氧化鈦及染料太陽能電池能有更進一步的了解。

另外感謝柏勳介紹了我一個有趣的休閒活動，也能在適時提供幫助。感謝王瑜讓我有機會跟別人說嘴我同學有在跨年演唱會上表演過。感謝雅婷在我心情低落時的給予鼓勵。感謝怡萱的星冰樂，需要的話我非常樂意再你借腳踏車。感謝兆權讓我知道台大附近原來有那麼多好吃的餐廳，猶記得去吃玫瑰與布朗尼那天的情景…，感謝宜婷讓我知道《天工開物》不僅僅是一部明朝的科學著作。另外還要感謝昆樺學長及昱瑩學姐在某次深夜的指導。

最後感謝我的家人的支持，讓我能在生活上無後顧之憂，也感謝支持我的所有朋友。大家給我的鼓勵及支持，在此萬分感謝。

摘要

溶液-凝膠法提供一種簡單的方式去改變材料的特性,例如:溫度、pH 值...等，在這個研究中我們藉由調控氧化鈦溶液的反應時間進而合成出具有不同氧鈦比之氧化鈦，其材料特性會將隨之而發生改變，氧鈦比不同時，材料的能帶會有所改變，當氧鈦比增加，則材料的導帶及價帶能階越靠近二氧化鈦，其中導帶能階從 3.92eV 變化至 4.32eV(二氧化鈦為 4.37eV)，價帶能階從 7.73eV 變化至 7.60eV(二氧化鈦價帶能階為 7.58eV)，藉由將之導入所作之有機太陽能電池中，不同氧鈦比之材料會對元件表現產生影響。而我們發現具有低氧鈦比的氧化鈦在元件上能有較好的表現，這是由於其導帶能階位置與電子受體的最低未占分子軌道(LUMO)形成較為適當的條件，能夠有利於電子傳輸。

另一方面，有機太陽能電池雖具有許多優點(例如：低成本、易於大面積製作等)，但元件在大氣下容易使效率衰退，則為一重大缺點。然而，藉由導入氧化鈦作為水氧阻擋層，可以很明顯的看到元件大氣穩定性大幅上升，即使在大氣下長時間使用仍可保有不錯的效率。

關鍵字：氧化鈦、有機太陽能電池

ABSTRACT

Sol-gel method provide an easy way to modify the characteristics of material. In this study, we synthesis titanium oxide with different O/Ti ratio by sol-gel method but not by reactive sputtering. The characteristics of titanium oxide with different O/Ti atomic ratio is quite different, The band gap change with O/Ti ratio, when increase the O/Ti ratio, the conduction and valence band level more approach to the band position of titanium dioxide. The conduction band level change from 3.92 to 4.32 eV (the conduction band level of titanium dioxide is 4.37 eV), and the valence band level change from 7.73 to 7.60 eV (the valence band level of titanium dioxide is 7.58 eV). By introducing the TiO_x into the device, the titanium oxide with the lowest O/Ti ratio is the best for electron transport layer of OPV, we consider that the conduction band level of TiO_x approach to the LUMO of electron acceptor, result in a good condition for electron transport.

On the other hand, the air stability is a serious problems for the development of OPVs. The performance of device without protective layer degraded in the air dramatically. However, by introducing TiO_x as a shielding layer, the device will remain high performance even storage in air for a long time.

Key words : titanium oxide 、 organic solar cell

CONTENTS

口試委員審定書	i
Acknowledgements	ii
摘要	iii
ABSTRACT	iv
CONTENTS	v
LIST OF FIGURES	viii
LIST OF TABLES	xii
Chapter 1 Introduction.....	1
1.1 Preface	1
1.2 Introduction for PV.....	1
1.2.1 Inorganic solar cell.....	1
1.2.2 Dye-sensitized solar cell	2
1.2.3 Organic/Polymer solar cell.....	3
1.3 Components of OPV.....	8
1.3.1 Active layer	8
1.3.2 Electrode	9
1.3.3 Hole transport layer.....	11
1.3.4 Electron transport layer	12
1.4 Research Motivation.....	14
1.5 Reference	15
Chapter 2 Experimental Setup	18
2.1 Solar Spectrum	18
2.2 Typical J-V Characteristic of solar cell.....	20

2.3	Atomic Force Microscope	22
2.4	UV-Visible absorption spectroscopy	23
2.5	Cyclic Voltammetry	24
2.6	AC Impedance Spectroscopy.....	26
2.7	X-ray Photoelectron Spectroscopy	27
2.8	Reference	28

Chapter 3 Preparation and Analysis of Titanium Oxide with Different O/Ti ratio

3.1	Introduction of Titanium Oxide	29
3.2	Sol-Gel Method	30
3.3	Synthesis Procedures of Titanium Oxide.....	33
3.4	Characteristics of Crystallinity, Particle Size and Atomic Ratio	35
3.4.1	X-ray Diffractometry.....	35
3.5	Determine the Energy Gap and Conduction Band Level of Titanium Oxide.....	40
3.5.1	UV-Visible spectroscopy	40
3.5.2	Cyclic voltammetry measurement.....	41
3.6	Reference	45

Chapter 4 The Performance of Device with Different Titanium Oxide as Electron Transport Layer.....

4.1	Fabrication of Polymer Solar Cell with Titanium Oxide.....	47
4.2	Device Performance with TiO _x Dispensed in Different Solvent	50
4.3	Device Performance with Different O/Ti Ratio	54
4.3.1	Device performance	54
4.3.2	The effect of band diagram	56
4.4	Air Stability of OPV with TiO _x	63

4.5	Summary.....	71
4.6	Reference	72
Chapter 5	Conclusions.....	74



LIST OF FIGURES

Fig. 1-1	Structure of inorganic solar cell. ^[1]	1
Fig. 1-2	The device structure of dye-sensitized solar cell (DSSC).	3
Fig. 1-3	The working principle of an organic solar cell.	4
Fig. 1-4	Single layer structure and its mechanism. The photogenerate exciton can only separate near the interface of cathode and polymer.	5
Fig. 1-5	Molecular structures of copper phthalocyanine (CuPc) and perylene tetracarboxylic derivative (PTC)	5
Fig. 1-6	In a donor-acceptor OPV light absorption creates excitons, which diffuse to the donor- acceptor interface, where dissociate into charge carriers, which drift toward the transparent conductive oxide (TCO) and Al electrodes.	6
Fig. 1-7	In a BHJ OPV, light enters through the transparent conductive oxide (TCO) electrode, generates excitons, which split into electron and hole at the donor-acceptor interface, and dissociate into charge carriers which drift toward the electrodes.	7
Fig. 1-8	Component for each layer in OPV.	8
Fig. 1-9	Molecule structure of P3HT and PCBM.	9
Fig. 1-10	Voc, FF, and normalized efficiency vs. negative electrode type ^[18]	10
Fig. 1-11	Molecule structure of PEDOT and PSS.	11
Fig. 1-12	Graphene oxide as hole transport layer in OPVs.	12
Fig. 1-13	By introduced ZnO as electron transport layer in inverted type OPV.	13
Fig. 2-1	Solar radiation spectrum ^[1]	18
Fig. 2-2	The path length of the solar radiation through the Earth's atmosphere in	

	units of Air Mass(AM) increase with the angle from zenith. ^[2]	19
Fig. 2-3	Characteristic of I-V curve	20
Fig. 2-4	Schematic illustration of absorption spectroscopy setup.....	23
Fig. 2-5	Typical cyclic voltammogram where i_{pc} and i_{pa} show the peak cathodic and anodic current respectively for a reversible reaction ^[3]	24
Fig. 2-6	Basic components of XPS system. ^[4]	27
Fig. 3-1	Mechanism of (a)hydrolysis (b) alcoxolation (c) oxolation (d)condensation	31
Fig. 3-2	Structure of Titanium(IV) isopropoxide(left) 2-methanoxyethanol(middle) 、 Ethanolamine(right).....	33
Fig. 3-3	Different reaction time of titanium oxide	34
Fig. 3-4	X-ray diffraction pattern of titanium oxide, as synthesis(top).....	35
Fig. 3-5	XPS quantification of atomic composition for reaction (a)3hrs 、 (b)6hrs 、 (c)9hrs.....	36
Fig. 3-6	Ti 2p XPS spectra of titanium oxide with different reaction time after deconvolution. Reaction for (a) 3hrs (b) 6hrs (c) 9hrs	38
Fig. 3-7	TEM image of titanium oxide(a)reaction time = 3hrs (b)6hrs (c) 9hrs	39
Fig. 3-8	Absorbance spectrum for different O/Ti ratio.	40
Fig. 3-9	Tauc plot of titanium oxide with different O/Ti ratio	41
Fig. 3-10	Cyclic voltammograms of titanium oxide with different O/Ti ratio low(left), medium(middle), high(right).	42
Fig. 3-11	Cyclic voltammograms and Tauc plot of TiO ₂	43
Fig. 3-12	Band diagram of titanium oxide with different O/Ti ratio.....	44
Fig. 4-1	Structure of the device with TiO _x	48
Fig. 4-2	The flow chart shows the procedure for preparing device.	48
Fig. 4-3	Band diagram of the device	49

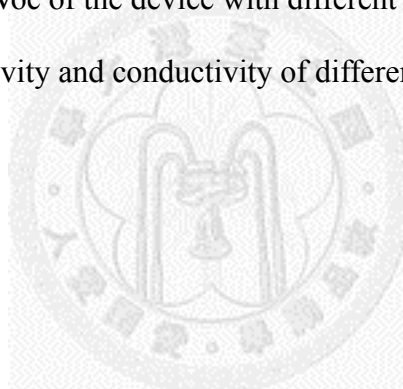
Fig. 4-4	Current-voltage characteristics of the polymer solar cells consisting of TiO_x as an electron transport layer. dilute in different solvent.....	51
Fig. 4-5	The morphology of titanium oxide dilute in different solvent.	52
Fig. 4-6	The phase image of titanium oxide dilute in different solvent.	53
Fig. 4-7	J-V curve of the device with different TiO_x	54
Fig. 4-8	External quantum efficiency spectra for devices with and without the TiO_x ...	55
Fig. 4-9	AFM image of titanium oxide with different O/Ti ratio (a)low O/Ti ratio(b)medium O/Ti ratio(c)high O/Ti ratio.....	56
Fig. 4-10	Corresponding energy level diagram of a device based on a $\text{TiO}_2\text{:Cs}$. ^[7] ...	58
Fig. 4-11	Two explanations of the origin of open current voltage	59
Fig. 4-12	The energy level of cathode.(a)modified by low O/Ti ratio, (b)modified by high O/Ti ratio.	59
Fig. 4-13	Ag/ TiO_x /Ag device structure	60
Fig. 4-14	I-V curve of the Ag- TiO_x -Ag device.....	61
Fig. 4-15	Atomic ratio O/Ti of oxygen to titanium (left-hand scale) and electrical conductivity (right-hand scale) as a function of the growth rate of TiO_x , films; lines drawn to guide the eye. ^[2]	62
Fig. 4-16	The TiO_x layer acts as a shielding and scavenging layer which prevents the intrusion of oxygen and humidity into the electronically active polymers ..	63
Fig. 4-17	Device performance as a function of storage time for polymer solar cells. The current density-voltage ($J-V$) characteristics of polymer solar cells with(a) and without the TiO_x layer(b)	65
Fig. 4-18	Comparison of the power conversion efficiencies as a function of storage time for polymer solar cells with and without the TiO_x layer	66
Fig. 4-19	the performance of device as a function of storage time for polymer solar	

cells with and without the TiO_x layer	67
Fig. 4-20 The nyquist plots of device (a)dark 、(b)light	68
Fig. 4-21 The nyquist plots of device (a) without _x (b) with TiO_x	69
Fig. 4-22 The R_p value of device as a function of irradiation time.	70



LIST OF TABLES

Table 1-1	Status of the power conversion efficiencies, as reached for inorganic solar cells and the technology used to prepare these solar cell ^[4]	2
Table 3-1	O/Ti atomic ratio for different reaction time.	37
Table 3-2	Summarized of the conduction and valence band level	43
Table 4-1	Summaries of the device performance of conventional polymer solar cells using TiO _x as electron transport layer dilute in different solvent.	50
Table 4-2	Summaries of the device performance of different O/Ti ratio.....	55
Table 4-3	Summaries the Voc of the device with different O/Ti ratio	59
Table 4-4	Electrical resistivity and conductivity of different titanium oxide	61



Chapter 1 Introduction

1.1 Preface

The oil, natural gas and coal are the main energy source. According to statistics, the global oil stockpiles left about 50 years, natural gas about 60 years, such as coal, nuclear energy etc. have its limit too.

The fossil oil accounted for more than 85% of the global energy consumption, it can be seen the dependence on fossil oil .In addition, the issue of global climate change, mainly due to massive emissions of carbon dioxide, the generated source of CO₂ is the combustion of fossil energy, therefore sustainable development of the Earth, reducing CO₂ emissions and improve the greenhouse effect is a global consensus.

In order to reduce CO₂ emissions, the solar energy is a promising potential alternative energy sources .The solar has many features, the distribution is broad and non-polluting. In a nutshell, the solar energy is a clean energy. The sun generate a huge amount of energy, the energy accepted by the sun is excess of thirty thousand times than we need each year. How to effectively access to solar energy as an energy source is an important issues.

1.2 Introduction for PV

1.2.1 Inorganic solar cell

The inorganic solar cells formed a p-n junction by doped semiconductor material, when light irritated the device, the electron – hole pairs generate in both n-type and p-type semiconductors, the generated electron and hole diffuse to the junction and separated by the build-in electric field, producing electrical current through the device.

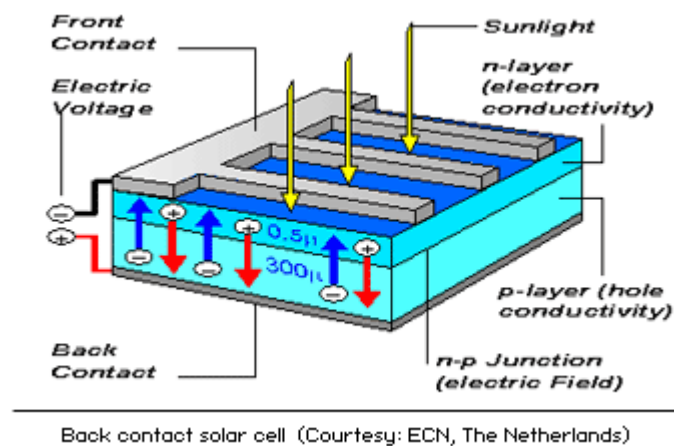


Fig. 1-1 Structure of inorganic solar cell.^[1]

The Bell Labs made the first inorganic solar cells in 1954 and the energy conversion efficiency is about 6%^[2], after years of research, the single crystalline silicon solar cells have demonstrated high-energy conversion efficiencies up to 24.7% in laboratory^[3]. Although the inorganic solar cells is good at high efficiency but the expensive price is a big problem.

Table 1-1 Status of the power conversion efficiencies, as reached for inorganic solar cells and the technology used to prepare these solar cell ^[4]

Semiconductor material	Power conversion efficiency [%]	Technology
Mono-crystalline silicon	20-24	Crystalline
Poly-crystalline silicon	13-18	Thick and thin-film
Gallium-arsenide	20-29	Crystalline
Amorphous silicon	8-13	Thin-film
Cadmium telluride	10-17	Thin-film
Cadmium indium selenide	10-19	Thin-film

1.2.2 Dye-sensitized solar cell

In a dye-sensitized solar cell, the organic dye molecules adsorbed at the surface of an inorganic wideband gap semiconductor is used for absorption of light and injection of the photoexcited electron into the conduction band of the semiconductor. After years of research, Grätzel and co-workers improved the efficiency of DSSC by using nanoporous titanium dioxide^[5], the porous structure provide high surface area so more dye molecules can adsorb to the titanium dioxide. Nowadays, ruthenium dye-sensitized solar cells reach an energy conversion efficiency of about 10% .

In the Grätzel cell, the ruthenium dye absorb light and the photoexcited electrons inject into the TiO₂ conduction band. An I⁻/I₃⁻ redox couple, contained in an organic solvent, is used to regenerate the photooxidized dye molecules. In the cells, the positive charge is transported by the liquid electrolyte to a metal electrode, where I₃⁻ catch an electron from counter electrode, while the negative charges injected in TiO₂ are collected at the fluorine doped tin oxide (SnO₂:F) electrode.

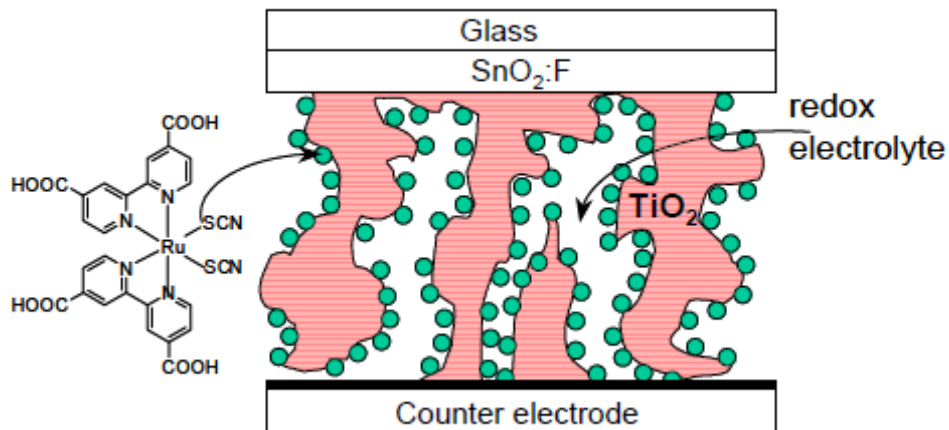


Fig. 1-2 The device structure of dye-sensitized solar cell (DSSC).

1.2.3 Organic/Polymer solar cell

Organic/Polymer solar cell have many features like low-cost, large-area, and flexible. To date, the best energy conversion efficiency of organic/polymer solar cell is about 5%^[6]. Organic/Polymer solar cell are composed of organic semiconductor. By definition, the material that absorbs the photon and generate electron-hole pairs called donor, the material accept the electron provided by donor called acceptor. When light irradiate the device, the donor generates strongly bounded electron-hole pairs, the strongly bounded electron-hole pairs are more localized in organic molecules which electrostatic attraction can keep the electron and hole together as a “exciton” that are bound at room temperature, if the excitons can’t be separated into free electron and hole efficiently before the recombination occur that will cause the low performance of the device. Therefore, in order to separate the excitons efficiently, an interface across which the chemical potential of electron decrease must be provided. Figure 1.3 shows a interface with the proper band alignment. The donor absorb a photon and generate an exciton. After that the exciton diffuses to the donor/acceptor interface within its lifetime. Then,

because of the different chemical potential across the interface, the exciton dissociation at the donor/acceptor interface. Afterward, the electron and hole transport to cathode and anode respectively.

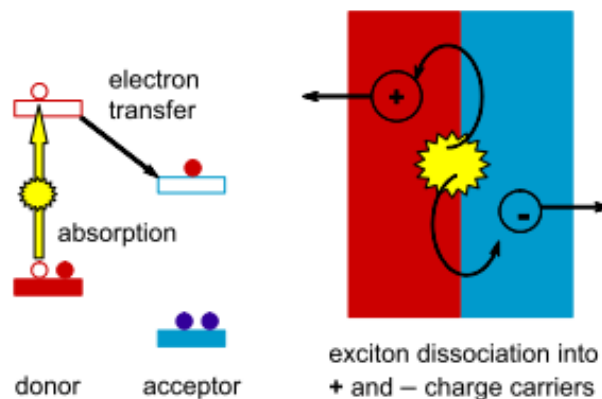


Fig. 1-3 The working principle of an organic solar cell. Light illuminate the donor through a transparent electrode result in an electron is promote from the highest occupied molecular orbital (HOMO) to the lowest unoccupied molecular orbital(LUMO) of the donor. Then, the excited electron transfer to the LUMO of acceptor and leave a hole in the donor. the electron and hole transport to cathode and anode respectively.^[7]

The evolution of the organic solar cell device structure, starting with single-layer structure, and then to double-layer structure, the final material mixed bulk-heterojunction.

Figure 1.4 shows the band diagram of single layer structure and the energy conversion efficiency is about 0.7%.^[8] The energy conversion efficiency for single layer structure is due to inefficiently charge separation and transport.

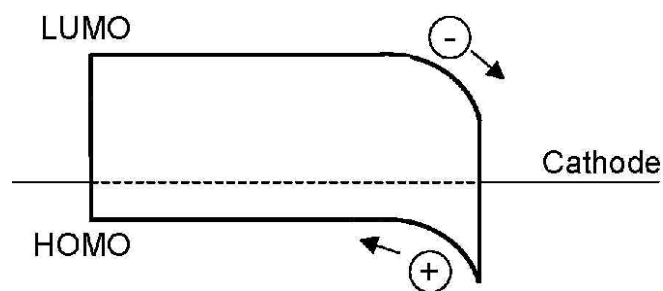


Fig. 1-4 Single layer structure and its mechanism. The photogenerated exciton can only separate near the interface of cathode and polymer.

The bi-layer heterojunction structure creates an interface to overcome the problem of inefficient charge separation and transport problems in single layer structure. In 1986, C.W Tang and his co-workers used a copper phthalocyanine (CuPc) as a donor and perylene derivative as an acceptor and the energy conversion efficiency is about 1%^[9]. Although the energy conversion efficiency is higher than single layer structure but the charge separation can only occur at the junction.

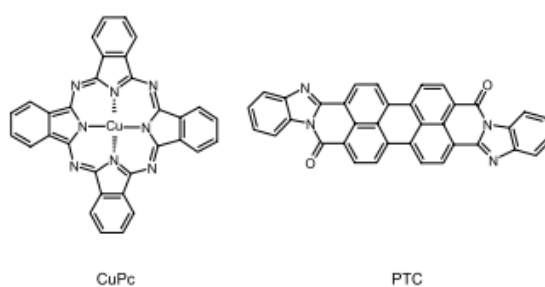


Fig. 1-5 Molecular structures of copper phthalocyanine (CuPc) and perylene tetracarboxylic derivative (PTC)

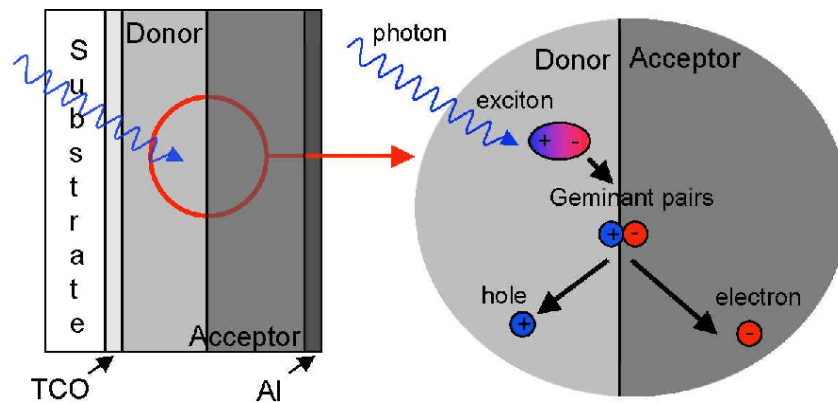


Fig. 1-6 In a donor-acceptor OPV light absorption creates excitons, which diffuse to the donor- acceptor interface, where dissociate into charge carriers, which drift toward the transparent conductive oxide (TCO) and Al electrodes.

In order to increase the interface to efficiently separate the excitations, the bulk-heterojunction structure has been proposed. By simple mixing the p and n-type materials and relying on the intrinsic tendency of polymer materials to phase separate on a nanometer dimension, junctions throughout the bulk of the material are created that ensure quantitative dissociation of photogenerated excitons. The bulk-heterojunction structure has been the most widely used photoactive layer. In 1994, G. Yu and A. J. Heeger used conjugate polymer blend C_{60} as active layer to fabricate the device. To date, the best efficiency for bulk-heterojunction structure is about 5%.^[10]

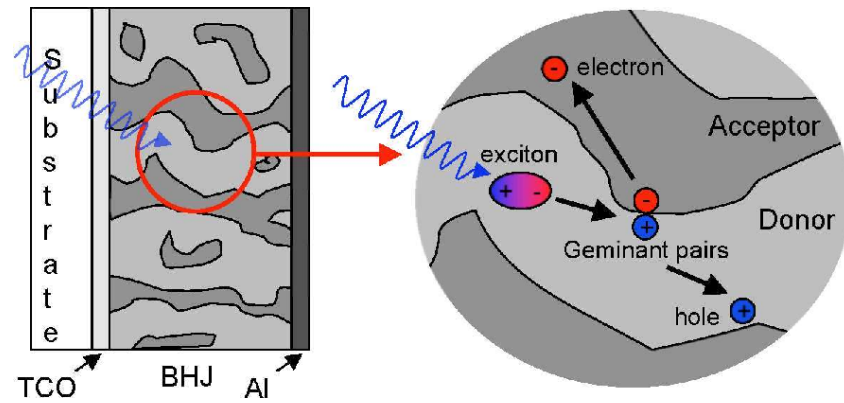


Fig. 1-7 In a BHJ OPV, light enters through the transparent conductive oxide (TCO) electrode, generates excitons, which split into electron and hole at the donor-acceptor interface, and dissociate into charge carriers which drift toward the electrodes.



1.3 Components of OPV

The organic solar cell can be divided into several parts,

Transparent electrode: Light irradiation side, need a transparent material.

Active layer: Absorb light and produce excitons.

Hole transport layer: Improved selectivity of the anode and smooth the surface.

Electron transport layer: Improved selectivity of the cathode and protect the active layer.

Here, we do a brief introduction for each layer.

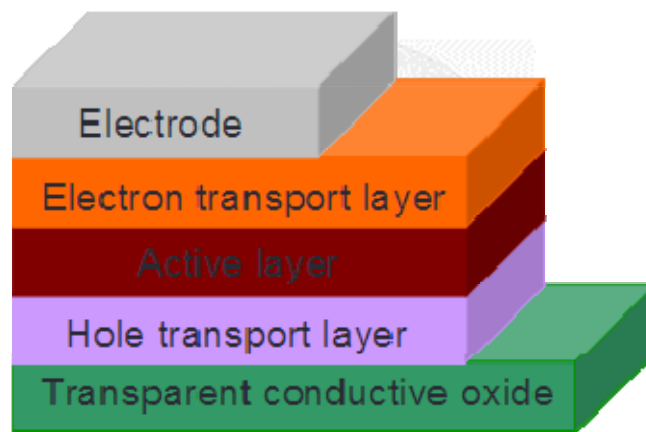


Fig. 1-8 Component for each layer in OPV.

1.3.1 Active layer

Several kinds of donors and acceptors materials have been utilized as active layer in the bulk-heterojunction solar cell. Up to now, the most suitable combination is a blend of an organic semiconductor as a donor and a C₆₀ derivatives, fullerene as acceptor. It is well established that at the interface of these materials a sub-picosecond photoinduced charge transfer occurs that ensures efficient charge generation.

So far, the most widely used combination is P3HT(Poly(3-hexylthiophene)) and

PCBM([6,6]-phenyl-C61-butyric acid methyl ester). In PCBM, the fullerene carries a substituent that prevents extensive crystallization upon mixing with the conjugated polymer and enhances the miscibility and P3HT which is known to have a high carrier mobility and low band gap compare to the material used before.

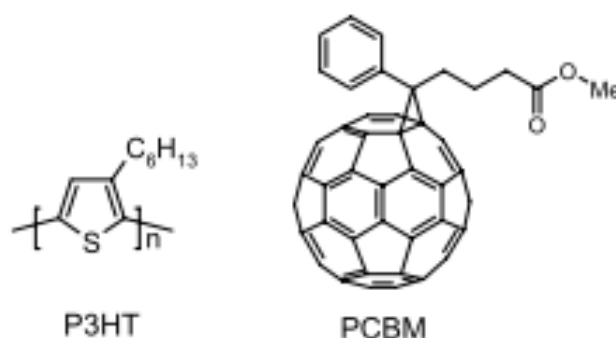


Fig. 1-9 Molecule structure of P3HT and PCBM.

1.3.2 Electrode

The electrode in OPV can divide into two parts, one is transparent conductive oxide (TCO), another is metal electrode.

Indium tin oxide (ITO, or tin-doped indium oxide) is one of the most widely used transparent conducting oxides. It can be deposited on substrate by E-beam evaporation, physical vapor deposition, or sputter. However, the amount of Indium is rare in earth so many other materials have been proposed. In recent years, graphene had been demonstrated a promising material for transparent electrode, due to its good conductivity and optical transparency.^[19,20]

Metals can be thermally evaporated to form a non-transparent or transparent electrode or/and interfacial layer. Al, Mg/Ag, Ca/Al, Ca/Ag, Ba/Al, Au were successfully used in OPV devices. A combination of a low work function metal (e.g. Ca, Ba) with Ag or Al is a common way to decrease the work function of the electrode and

to prevent Ag and Al atoms from diffusing into the photoactive layer. The work function of these metals ranges from 5.1 eV (Au) to 2.7eV (Ba).

Fig. 1.12 shows the experimental results for several electrode materials as cathodes in the normal device structure (ITO/PEDOT:PSS/P3HT:PCBM/cathode). Voc, FF and the normalized efficiency is depicted. The pristine metals Al and Ag have the lowest performance while in combination with Mg : Ag, LiF, Ba or Ca the device performance is clearly improved because these materials decrease the work function of the cathode, act as protection layer and improve the carrier selectivity.

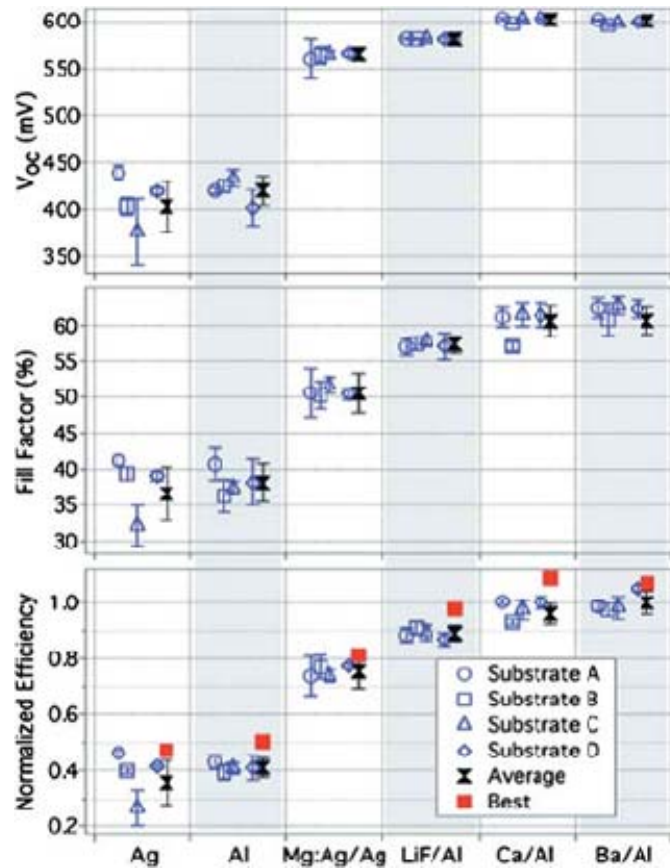


Fig. 1-10 Voc, FF, and normalized efficiency vs. negative electrode type ^[18]

1.3.3 Hole transport layer

PEDOT (poly(3,4-ethylenedioxythiophene)) is widely used conducting polymer as a hole transport layer and transparent electrode material in organic electronic devices. Usually PEDOT is doped with PSS (poly(styrenesulfonate)) for improved conductivity and solubility. In the device, PEDOT:PSS can improved selectivity of the anode, smooth the TCO (e.g. ITO) and modified the work function of the transparent electrode. However PEDOT:PSS is highly acidic ($\text{pH} \sim 1$) and corrodes ITO that will deteriorate the device[11]. Several p-type metal oxide has been introduce into organic solar cell successfully such as V_2O_5 、 MoO_3 、 WO_3 .^[12-14] However these material need to use thermal evaporation process which is not compatible with solution process.

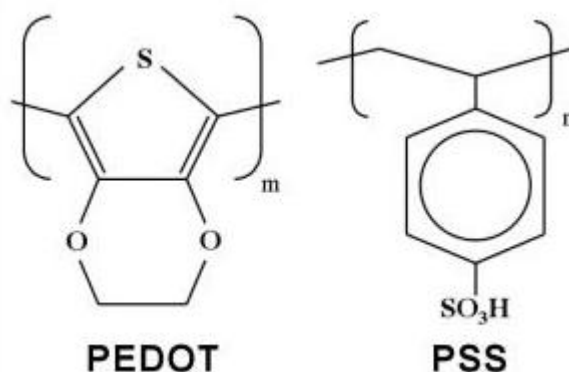


Fig. 1-11 Molecule structure of PEDOT and PSS.

In recent years, the materials based on carbon is very popular and graphene oxide (GO) is one of promising material utilizing in organic solar cell. In 2010, C. W. Chen and co-worker utilized GO as hole transport layer in OPVs^[15] and the device exhibits power conversion efficiency of 3.5%, the efficiency is comparable to device fabricated with PEDOT:PSS and the GO is compatible with solution process

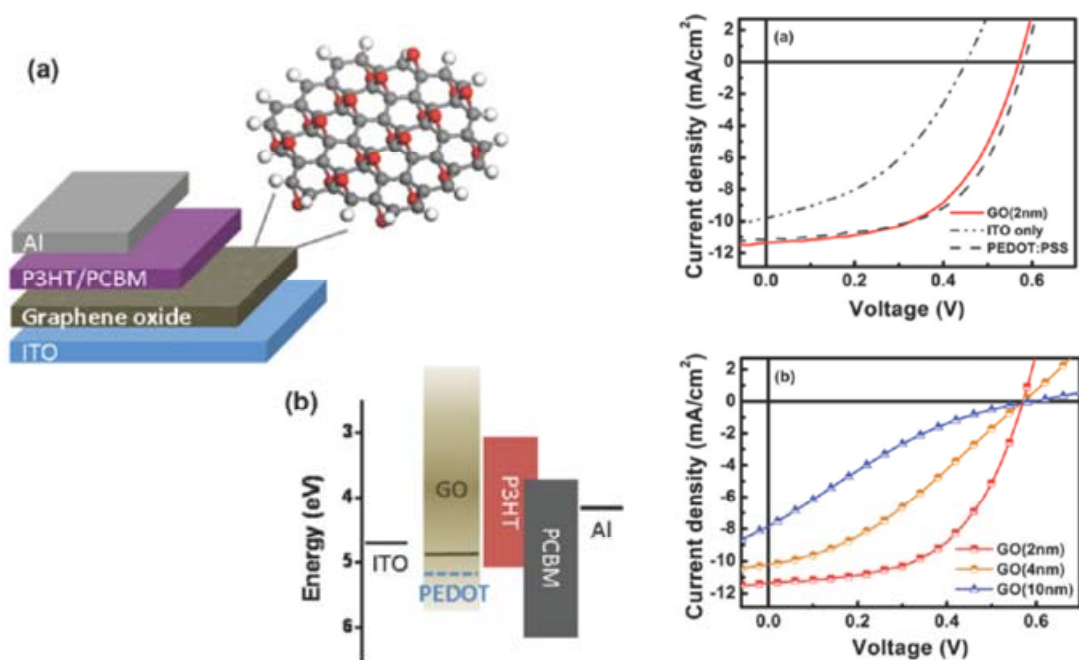


Fig. 1-12 Graphene oxide as hole transport layer in OPVs.

1.3.4 Electron transport layer

For an n-type material which facilitates electron transfer from the LUMO of the acceptor to the conduction band of the metal oxide. In recent years, zinc oxide (ZnO) has been introduced into OPV devices as the electron transport layer because of its high electron mobility. Kyaw *et al.* prepared a ZnO electron selective layer by a sol-gel process in an inverted OPV device on a glass substrate and achieve a PCE of 3.09%.^[16]

There are few materials can be an electron transport layer for conventional type photovoltaic and also compatible to the solution process at the same time. Titanium oxide (TiO_x) as an electron transport layer has been proposed, the device performance obtain significantly improved.

Alkali metal salts such as caesium carbonate (Cs₂CO₃) is required to modify the work function of TCO for electron collecting., inverted OPV devices With Cs₂CO₃ exhibit

power conversion efficiency of 4% was demonstrated.^[17] However, Cs_2CO_3 exhibits deliquescence which affects severely the lifetime of OPV devices.

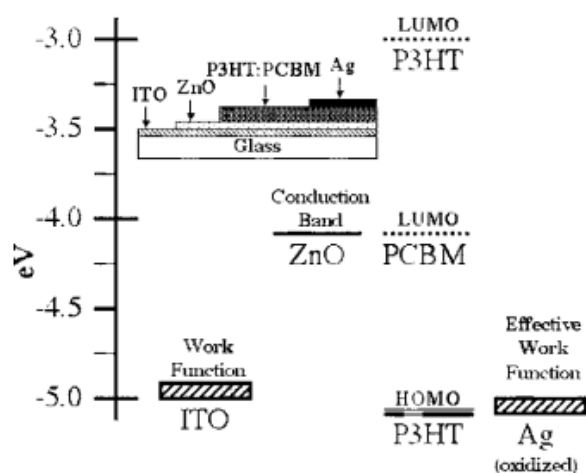
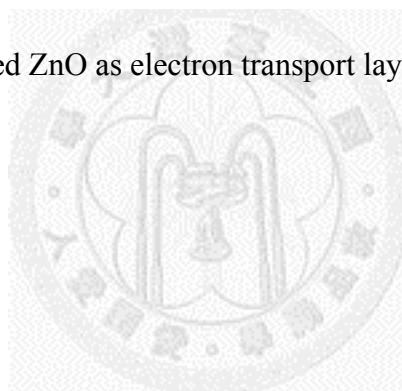


Fig. 1-13 By introduced ZnO as electron transport layer in inverted type OPV



1.4 Research Motivation

Although, there are many advantages of OPV, the power conversation of OPV is still lower than the inorganic solar cell and the stability is really bad. In recent years, how to improve the device performance have been widely studied. By introducing electron transport layer, we can improve the device performance and air stability at the same time. Sol-gel method provides a easy way to modify the characteristic of material. We try to modify the titanium oxide and find a better condition for the material.



1.5 Reference

- [1] Li, L.; Coates, N.; Moses, D., Solution-Processed Inorganic Solar Cell Based on in Situ Synthesis and Film Deposition of CuInS₂ Nanocrystals. *Journal of the American Chemical Society* **2009**, *132* (1), 22-23.
- [2] D.M Chapin, C. S. Fuller, and G.L. Pearson, "A New Silicon pn junction Photocell for Converting Solar Radiation into Electrical Power." *J.Appl. Phys.* 25, 676 (1954).
- [3] J. Zhao, A. Wang, and M. A. Green, "24.5% efficiency silicon PERT cells on MCZ substrates and 24.7% efficiency PERL cells on FZ substrates," *Prog. Photovolt. : Res. Appl.* 7, 471 (1999)
- [4] Photovoltaic Network for the Development of a Roadmap for PV (PV-NET).
- [5] Ito, S.; Murakami, T. N.; Comte, P.; Liska, P.; Grätzel, C.; Nazeeruddin, M. K.; Grätzel, M., Fabrication of thin film dye sensitized solar cells with solar to electric power conversion efficiency over 10%. *Thin Solid Films* **2008**, *516* (14), 4613-4619.
- [6] Li, G.; Shrotriya, V.; Huang, J.; Yao, Y.; Moriarty, T.; Emery, K.; Yang, Y., High-efficiency solution processable polymer photovoltaic cells by self-organization of polymer blends. *Nat Mater* **2005**, *4* (11), 864-868.
- [7] Photophysics of Molecules and Materials for Polymer Solar Cells, Paulus Albertus-van Hal
- [8] Coakley, K. M.; McGehee, M. D., Conjugated Polymer Photovoltaic Cells. *Chemistry of Materials* **2004**, *16* (23), 4533-4542.
- [9] Tang, C. W., Two-layer organic photovoltaic cell. *Applied Physics Letters* **1986**, *48* (2), 183-185.
- [10] Park, S. H.; Roy, A.; Beaupre, S.; Cho, S.; Coates, N.; Moon, J. S.; Moses, D.; Leclerc, M.; Lee, K.; Heeger, A. J., Bulk heterojunction solar cells with internal

- quantum efficiency approaching 100%. *Nat Photon* **2009**, 3 (5), 297-302.
- [11] Jung, J.; Kim, D. L.; Oh, S. H.; Kim, H. J., Stability enhancement of organic solar cells with solution-processed nickel oxide thin films as hole transport layers. *Solar Energy Materials and Solar Cells* **2012**, 102 (0), 103-108.
- [12] Chen, C.-W.; Lu, Y.-J.; Wu, C.-C.; Wu, E. H.-E.; Chu, C.-W.; Yang, Y., Effective connecting architecture for tandem organic light-emitting devices. *Applied Physics Letters* **2005**, 87 (24), 241121-241121-3.
- [13] Yook, K. S.; Lee, J. Y., Low driving voltage in organic light-emitting diodes using MoO₃ as an interlayer in hole transport layer. *Synthetic Metals* **2009**, 159 (1–2), 69-71.
- [14] Meyer, J.; Hamwi, S.; Bulow, T.; Johannes, H. H.; Riedl, T.; Kowalsky, W., Highly efficient simplified organic light emitting diodes. *Applied Physics Letters* **2007**, 91 (11), 113506-113506-3.
- [15] Li, S.-S.; Tu, K.-H.; Lin, C.-C.; Chen, C.-W.; Chhowalla, M., Solution-Processable Graphene Oxide as an Efficient Hole Transport Layer in Polymer Solar Cells. *ACS Nano* **2010**, 4 (6), 3169-3174.
- [16] Kyaw, A. K. K.; Sun, X. W.; Jiang, C. Y.; Lo, G. Q.; Zhao, D. W.; Kwong, D. L., An inverted organic solar cell employing a sol-gel derived ZnO electron selective layer and thermal evaporated MoO₃ hole selective layer. *Applied Physics Letters* **2008**, 93 (22), 221107-3.
- [17] Lee, Y.-I.; Youn, J.-H.; Ryu, M.-S.; Kim, J.; Moon, H.-T.; Jang, J., Electrical properties of inverted poly(3-hexylthiophene): Methano-fullerene [6,6]-phenyl C71-butyric acid methyl ester bulk hetero-junction solar cell with Cs₂CO₃ and MoO₃ layers. *Solar Energy Materials and Solar Cells* **2011**, 95 (12), 3276-3280.
- [18] Steim, R.; Kogler, F. R.; Brabec, C. J., Interface materials for organic solar cells.

Journal of Materials Chemistry **2010**, 20 (13), 2499-2512.

- [19] Li, X.; Zhu, Y.; Cai, W.; Borysiak, M.; Han, B.; Chen, D.; Piner, R. D.; Colombo, L.; Ruoff, R. S., Transfer of Large-Area Graphene Films for High-Performance Transparent Conductive Electrodes. *Nano Letters* **2009**, 9 (12), 4359-4363.
- [20] Wang, X.; Zhi, L.; Tsao, N.; Tomović, Ž.; Li, J.; Müllen, K., Transparent Carbon Films as Electrodes in Organic Solar Cells. *Angewandte Chemie* **2008**, 120 (16), 3032-3034.



Chapter 2 Experimental Setup

2.1 Solar Spectrum

The spectrum of the Sun's solar radiation is close to that of a black body with a temperature of about 5,800 K. As it passes through the atmosphere, sunlight is attenuated by scattering and absorption; the more atmosphere through which it passes, the greater the attenuation. As the sunlight travels through the atmosphere, chemicals interact with the sunlight and absorb certain wavelengths.

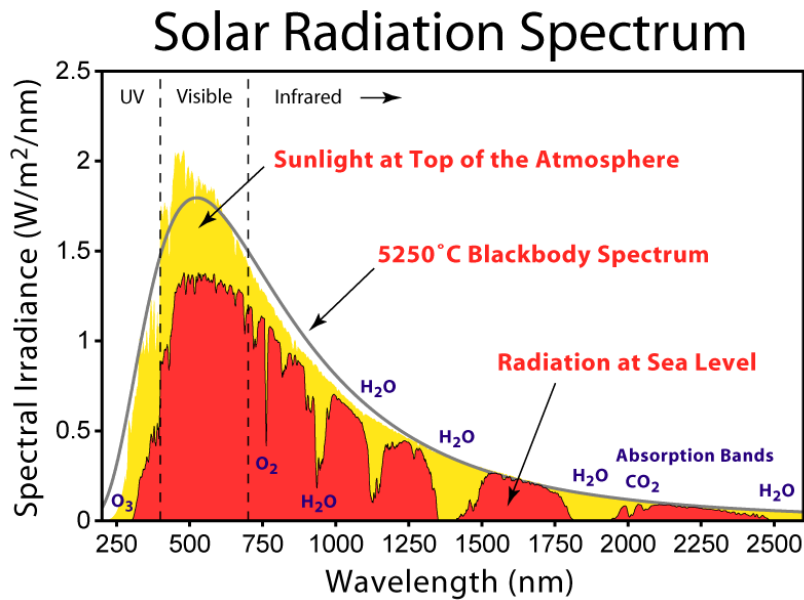


Fig. 2-1 Solar radiation spectrum^[1]

The air mass coefficient defines the direct optical path length through the Earth's atmosphere, expressed as a ratio relative to the path length vertically upwards, i.e. at the zenith.

$$AM = \frac{L}{L_0} = \frac{1}{\cos \theta}$$

Here, L_0 the zenith path length (i.e. normal to the Earth's surface) at sea level and θ is the zenith angle in degrees.

Solar panels do not generally operate under exactly one atmosphere's thickness: if the sun is at an angle to the Earth's surface the effective thickness will be greater. An AM number representing the spectrum at mid-latitudes is therefore much more common. "AM1.5", 1.5 atmosphere thickness, corresponds to a solar zenith angle of $\theta=48.2^\circ$. While the summertime AM number for mid-latitudes during the middle parts of the day is less than 1.5, higher figures apply in the morning and evening and at other times of the year. Therefore AM1.5 is useful to represent the overall yearly average for mid-latitudes. Consequently, the solar industry uses AM1.5 for all standardized testing of terrestrial solar panels.

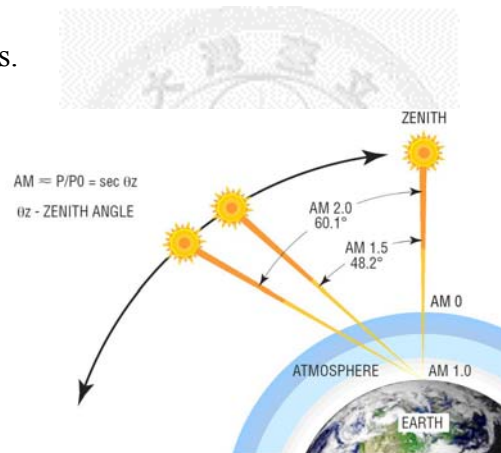


Fig. 2-2 The path length of the solar radiation through the Earth's atmosphere in units of Air Mass(AM) increase with the angle from zenith.^[2]

To analyze the device performance of photovoltaic, a Newport-Oriel solar simulator simulating AM 1.5 sun spectrum was used to illuminate from the transparent side of the device. Then, the I-V characteristics were recorded by Keithley 2410 sourcemeter unit.

In order to investigate the characterization of the solar cell, the current-voltage (I-V) curve in dark and illuminating are consider. The basic parameter in solar cell are short-circuit current(I_{sc})、open voltage(V_{oc})、fill factor(FF)、power conversion efficiency(PCE). Fig. 2.3 shows a typical I-V curve of a solar cell in dark and illumination.

2.2 Typical J-V Characteristic of solar cell

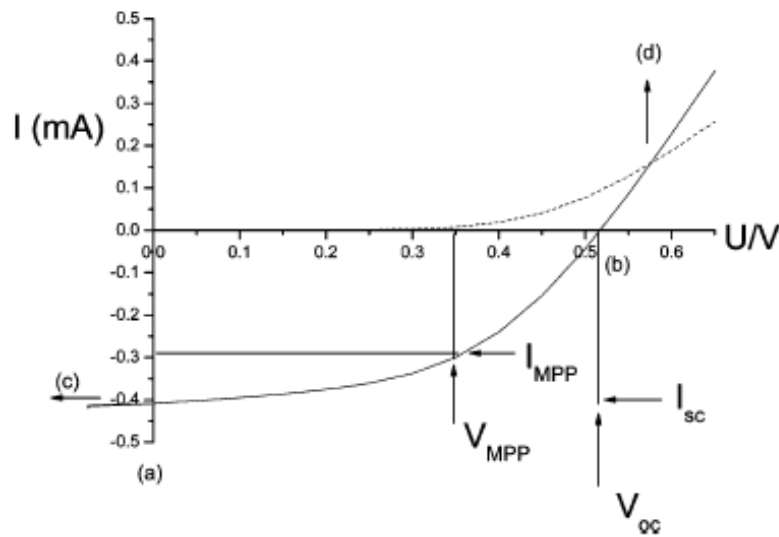


Fig. 2-3 Characteristic of I-V curve

Short circuit current(I_{sc})

From I-V curve, The definition of short current is the current when we apply zero voltage to the device. Fig. 2.3, point c represent the short circuit current. If the leakage current is not exist, the short circuit current equal to photocurrent.

Open circuit voltage(V_{oc})

Generally, the open circuit voltage is determined by the difference in work functions

of the two metal contacts. In organic solar cells, the open circuit voltage is found to be linearly dependent on the highest occupied molecular orbital HOMO level of the donor (p-type semiconductor quasi Fermi level) and lowest unoccupied molecular orbital LUMO level of the acceptor (n-type semiconductor quasi Fermi level).

Charge carrier losses at electrodes lower the Voc. Open circuit voltage is also affected by the morphology of the active layer in the polymer fullerene bulk- heterojunction solar cells.

Fill factor(FF)

The fill factor(FF) of solar cells is determined by

$$FF = \frac{I_{MPP} \times V_{MPP}}{I_{SC} \times V_{OC}}$$

where I_{MPP} and V_{MPP} are the current and voltage at the maximum power point of I-V curve in the fourth quadrant. The fill factor perform the diode properties of the solar cell. In general, large serial resistance(R_s) and small parallel(R_{sh}) will decrease the fill factor. By modifying the quality of the ohmic contact between polymer and metallic electrode can improve the fill factor. Introducing an inorganic metal salt like LiF will reduce the interface barrier at the interface barrier have been demonstrate.

Power conversion efficiency(PCE)

The definition of power conversion efficiency is the maximum output power divide to the power of the incident light.

$$\eta = \frac{P_{max}}{P_{in}} = \frac{FF \times V_{OC} \times I_{SC}}{P_{in}}$$

2.3 Atomic Force Microscope

The Atomic Force Microscope (AFM) is used to image the surface topography of a sample down to sub-nanometer scale. The AFM however requires no conductivity; here tip sample interactions are based on mechanical short or long-range forces.

The basic setup of an AFM consists of a measuring unit, a controller and a computer, which is collecting the data. To accomplish a full image, the sample is scanned line-by-line over a rectangular area with typically some few hundred lines using a sharp tip. There are three basic measurement modes for the AFM: Contact mode, non-contact mode and tapping mode. The difference of which lies in the different tip sample interaction used to control a constant distance between tip and sample. In the contact mode the tip is touching the sample with a certain pressure, leading to a bending of the cantilever at which end the tip is mounted. Both the non-contact and tapping mode use extended tip sample interaction via van der Waals long-range forces over several nm distances.

For soft organic materials the tapping mode offers destruction less measurement at high resolutions. In the case of tapping or non-contact mode, a quartz piezo is used to excite the cantilever to oscillations. The amplitude of these oscillations is depending on the interactions with the sample surface and is basically the more damped the closer the tip approaches to the surface. To keep a constant distance to the surface, the feedback loop maintains constant amplitude of the cantilever oscillation, which lies typically between 20 and 100 nm for the tapping mode and less for the non-contact mode. The amplitude is detected via a reflected laser spot onto a split photodiode detector, and the controller electronics applies a corresponding correction signal to the z-piezo of the scanner.

2.4 UV-Visible absorption spectroscopy

UV-Visible absorption spectra were recorded by a Jasco UV-Visible System. Before the measurement, we correct the baseline to normalize the incident light. Then, the sample and the reference glasses were put into each holder as illustrated in Fig. 2.4

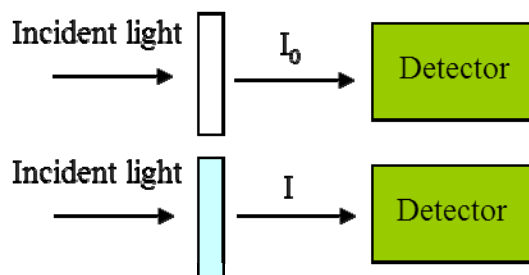


Fig. 2-4 Schematic illustration of absorption spectroscopy setup

The absorbance(A) and transmittance(T) are defined as :

$$T = \frac{I}{I_0}$$

$$A = -\log T = -\log\left(\frac{I}{I_0}\right)$$

Where I and I_0 are the intensity of light at a certain wavelength passing through the sample and reference, respectively. The absorption spectra were obtained by plotting A as a function of wavelength.

2.5 Cyclic Voltammetry

Cyclic voltammetry is a type of electrochemical measurement. In a cyclic voltammetry experiment the working electrode potential is ramped linearly versus time like linear sweep voltammetry. Cyclic voltammetry takes a step further than linear sweep voltammetry which ends when it reaches a set potential. When cyclic voltammetry reaches a set potential, the working electrode's potential slope is inverted. The change of slope can happen several times during the experiment. The current at the working electrode is plotted versus the applied voltage. Cyclic voltammetry is generally used to study the electrochemical properties

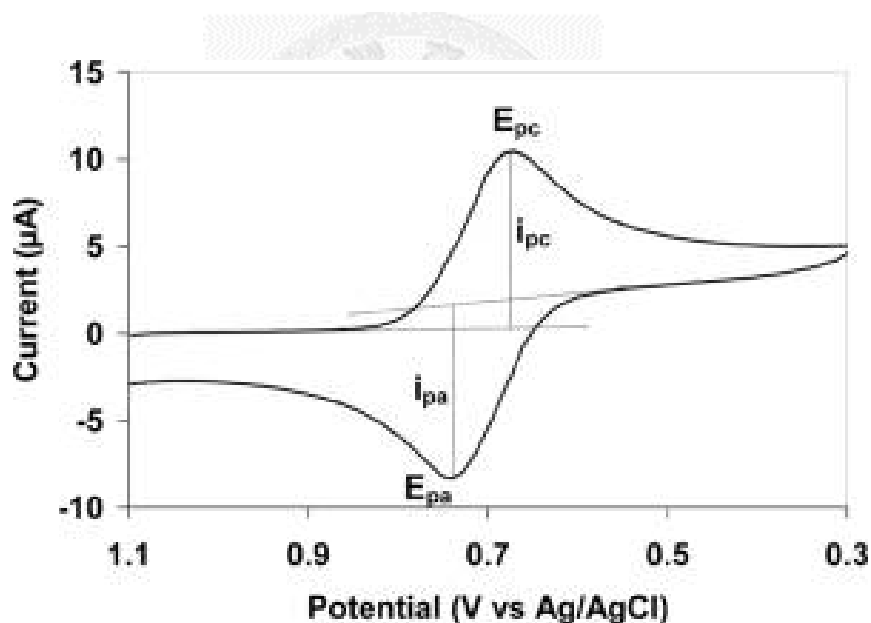


Fig. 2-5 Typical cyclic voltammogram where i_{pc} and i_{pa} show the peak cathodic and anodic current respectively for a reversible reaction ^[3]

Cyclic voltammetry experiments are typically carried out in a three electrochemical cell consisting of a platinum working electrode, a platinum counter electrode and a silver-silver chloride (Ag/AgCl) reference electrode. Because the onset values for

oxidation and reduction potentials of a reactant are determined versus Ag/AgCl. The redox couple ferrocene/ferricenium ion (Fc/Fc^+) was used as external standard. The estimations were done with the relation given as follows

$$Ec = [-e(E_{\text{onset(vs. Ag / AgCl)}} - E_{(\text{Fc} / \text{Fc}^+ \text{ vs. Ag / AgCl})})] - 4.8eV$$

where includes the ferrocene value of -4.8Ev with respect to the vacuum level.



2.6 AC Impedance Spectroscopy

Impedance spectroscopy, and also known as electrochemical impedance spectroscopy (EIS), measures the dielectric properties of the materials. It is based on the interaction of an external field with the electric dipole moment of the sample, often expressed by permittivity.

This technique measures the impedance of a system over a range of frequencies, and therefore the frequency response of the system, including the energy storage and dissipation properties, is revealed. Often, the data obtained by EIS is expressed graphically in a Bode plot or a Nyquist plot.

Impedance is the opposition to the flow of alternating current (AC) in a complex system. A passive complex electrical system comprises both energy dissipater (resistor) and energy storage (capacitor) elements. If the system is purely resistive, then the opposition to alternating current (AC) or direct current (DC) is simply resistance. Almost any physico-chemical system, such as dye-sensitized solar cell, organic solar cell, oscillators and even biological tissue possesses energy storage and dissipation properties. EIS examines them.

This technique has grown quickly in stature over the past few years and is now being widely employed in a wide variety of scientific fields such as fuel cell testing, biomolecular interaction, and microstructural characterization.

2.7 X-ray Photoelectron Spectroscopy

X-ray photoelectron spectroscopy (XPS) is a quantitative spectroscopic technique that measures the elemental composition, chemical state and electronic state of the elements that exist within a material. XPS spectra are obtained by irradiating a material with a beam of X-rays while simultaneously measuring the kinetic energy and number of electrons that escape from the top 1 to 10 nm of the material being analyzed. XPS requires ultra-high vacuum (UHV) conditions.

XPS is a surface chemical analysis technique that can be used to analyze the surface chemistry of a material, or after some treatment, for example: fracturing, cutting or scraping in air or UHV to expose the bulk chemistry, ion beam etching to clean off some of the surface contamination, exposure to heat to study the changes due to heating, exposure to reactive gases or solutions, exposure to ion beam implant, exposure to ultraviolet light.

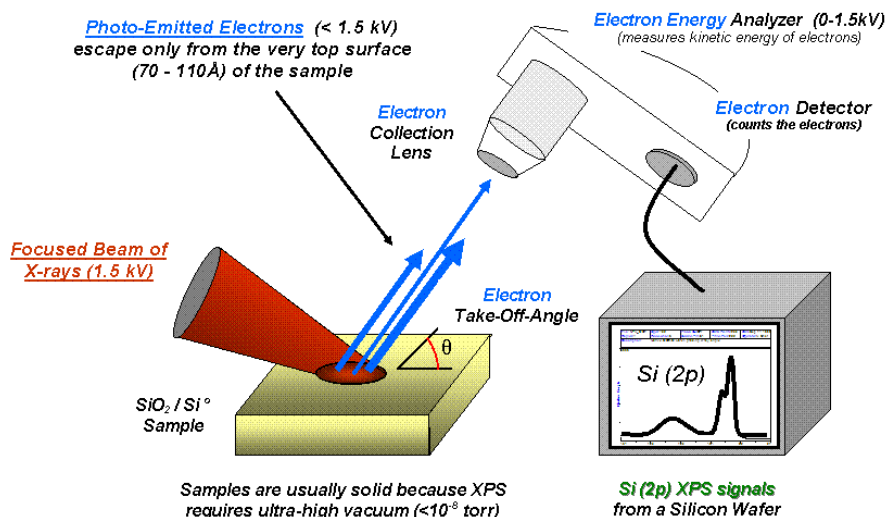


Fig. 2-6 Basic components of XPS system.^[4]

2.8 Reference

- [1] H. E. Hinteregger, Space Science Reviews **4** (4), 461 (1965).
- [2] Dommen, J.; Prévôt, A. S. H.; Hering, A. M.; Staffelbach, T.; Kok, G. L.; Schillawski, R. D., Photochemical production and aging of an urban air mass. *J. Geophys. Res.* **1999**, *104* (D5), 5493-5506.
- [3] Nguyen, T. A.; Kokot, S.; Ongarato, D. M.; Wallace, G. G., The Use of Cyclic Voltammetry and Principal Component Analysis for the Rapid Evaluation of Selectivity of Conductive Polymer Sensors. *Electroanalysis* **2000**, *12* (2), 89-95.
- [4] Principle of X-ray Photoemission Spectroscopy (XPS), and its application, *Faramarz S. Gard*



Chapter 3 Preparation and Analysis of Titanium Oxide with Different O/Ti ratio

Titanium oxide prepared by sol-gel method is a promising material as an electron transport layer in conventional type photovoltaic. Sol-gel method is easy to control materials by modulation of reaction conditions e.g. temperature, pH, etc.

Here, by control the synthetic variables, we prepare the titanium oxide with different O/Ti ratio.

3.1 Introduction of Titanium Oxide

A.J. Heeger et al. synthesis TiO_x by sol-gel method, introduce TiO_x into bulk-heterjunction OPV and enhanced the device performance successfully.^[13] The use of TiO_x provides several opportunities; specifically, the TiO_x layers enable higher performance from single cells, longer lifetime as a result of prevented the intrusion of oxygen and water vapor^[14], and the fabrication of the tandem cell architecture^[15]

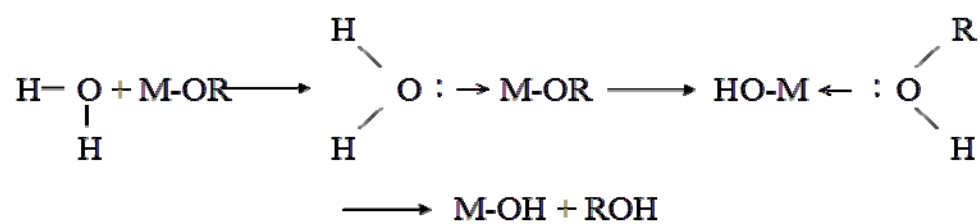
The TiO_x functions as an electron transport layer. Owing to the oxygen deficiency, the TiO_x layer is n-type doped. As a result, the inclusion of the TiO_x layer between the charge-separating layer and the aluminum cathode does not result in an increase in the series resistance^[16]. Moreover, since the conduction band level match to the Fermi energy of aluminum, there is facile electron transfer from the TiO_x electron transport layer to the aluminum cathode. Moreover, the TiO_x functions as a hole-blocking layer since the valence band level of TiO_x is sufficiently electronegative and below the HOMO of electron acceptor, to block holes.

3.2 Sol-Gel Method

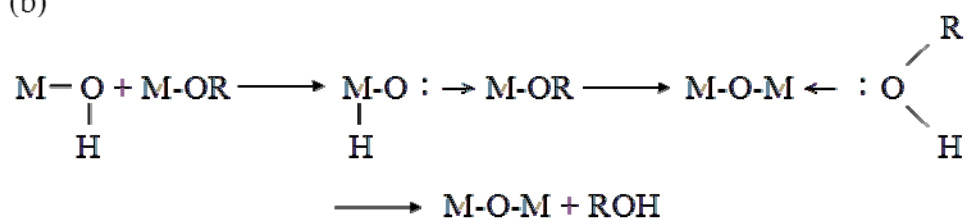
A colloid is a suspension in which the dispersed phase is so small ($\sim 1\text{-}1000\text{nm}$) that gravitational forces are negligible and interaction are dominated by short-range forces such as van der Waals attraction and surface charges. A sol is a colloidal suspension of solid particles in a liquid, these type of colloids can be used to generate particles from which ceramic materials can be made^[1].

In the sol-gel process the precursors (starting compounds) for preparation of a colloid consist of a metal or metalloid element surrounded by various ligands. Transition metal alkoxides, $M(OR)_z$, are widely used as molecular precursor to glasses and ceramics. Metal alkoxides are in general very reactive due to the presence of highly electronegative OR groups that stabilize $M^{[2]}$. For coordinatively saturated metals in the absence of catalyst, hydrolysis and condensation both occur, then followed by proton transfer from the attacking molecule to an alkoxo or hydoroxyo-ligand within the transition state and removed of the protonated as either alcohol(alcoxolation) or water(oxolation)^[3,4]. (mechanism of sol-gel method be depicted in figure 4.1)

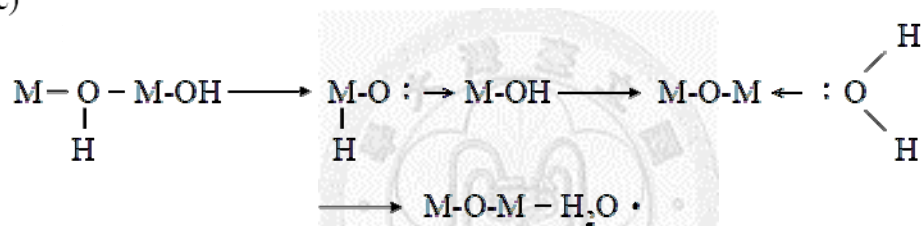
(a)



(b)



(c)



(d)

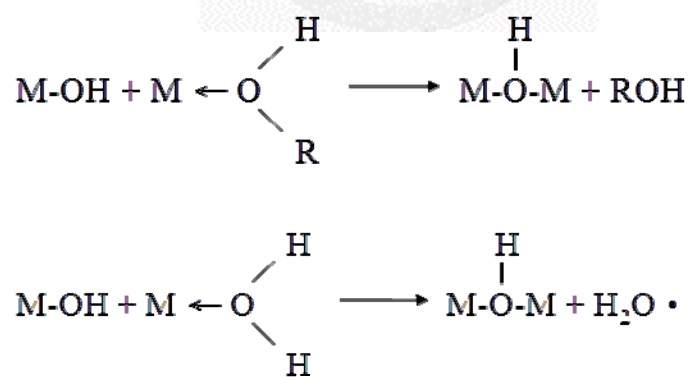


Fig. 3-1 Mechanism of (a)hydrolysis (b) alcoxolation (c) oxolation (d)condensation

There are many potential application of sol-gel-derived materials. Applications for sol-gel processing derive from the various state (e.g. films, fibers and powers). There are many advantages of sol-gel process, such as better homogeneity from raw materials, lower temperature of preparation, select the appropriate conditions can be prepared a variety of new materials...etc.

Films and coatings represent the application of sol-gel process^[5]. Thin films formed by dipping or spinning and may be processed quickly without cracking. The early applications for sol-gel films were in optical coatings as reviewed by Schroder^[6]. Since then, many new used for sol-gel films have been proposed in electronic, protective...etc. Livage and coworker have reviewed the electronic properties of transition metal oxide by sol-gel method, including titania, vanadia, and tungsten oxide.^[7,8] Protective film^[9] impact corrosion, promote adhesion, or provide planarization. Electronic passivation of a surface requires a dense, high-purity, pin-hole free film exhibiting high dielectric strength, low conductivity, and low surface state densities. In silicon-based microelectronics applications, sol-gel films are a low-temperature alternative to thermal SiO₂^[10].

3.3 Synthesis Procedures of Titanium Oxide

Chemicals:

Titanium(IV) isopropoxide: $\text{Ti}(\text{OCH}(\text{CH}_3)_2)_4$ purum grade 98%

2-methoxyethanol: purum grade 98%

Ethanolamine: purum grade 98%

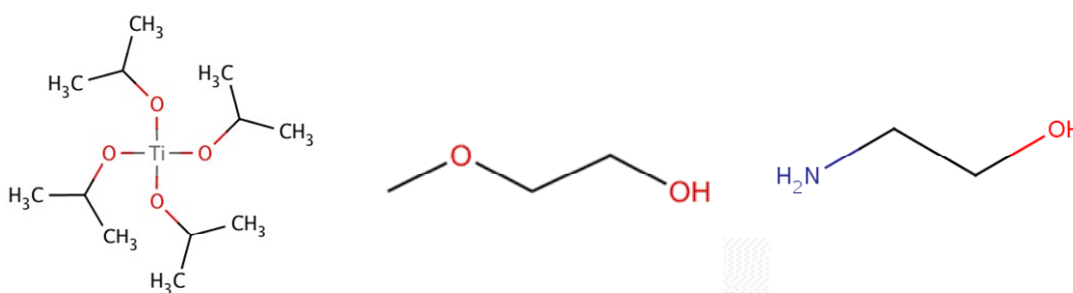


Fig. 3-2 Structure of Titanium(IV) isopropoxide(left) 2-methoxyethanol(middle) 、 Ethanolamine(right)

Apparatus:

Four-neck flask (250ml) 、 L-shape valve 、 Celsius thermometer 、 cork 、 agitator 、 reflux condenser

Methods:

- I. Add 50ml 2-methoxyethanol into a 250ml four-neck flask and put a small agitator of size about 2.5cm in length into the four-neck flask.
- II. Stir the agitator and add 10ml Titanium(IV) isopropoxide slowly to the four-neck flask to avoid the temperature increases dramatically. After a while, 5ml ethanolamine was added.

- III. Slowly raise the temperature of the system to 80°C for 2 hours under high purity argon flow in order to get rid of oxygen and water molecules.
- IV. After 2 hours, the solution was heated to 120°C for 1 hour.
- V. Repeat the thermal procedure(80°C and 120°C).
- VI. Turn off the hot plate, when the system was cooled down to room temperature, the final product solution was collected by pouring them into a jar which can be sealed later.

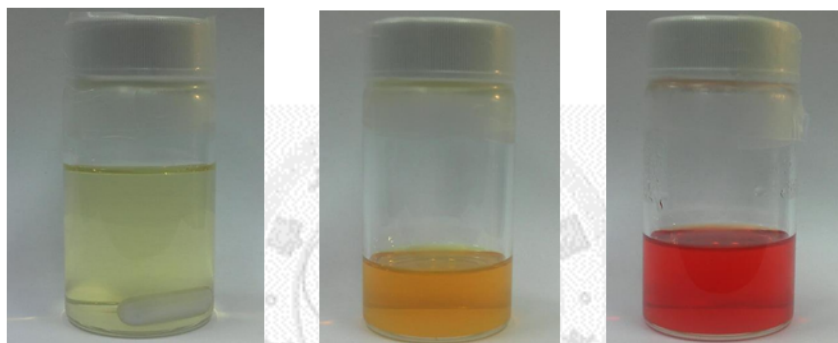


Fig. 3-3 Different reaction time of titanium oxide
3hrs(left) 、6hrs(middle) 、9hrs(right)

3.4 Characteristics of Crystallinity, Particle Size and Atomic Ratio

3.4.1 X-ray Diffractometry

X-ray diffractometry (XRD) investigate the crystal structure of the titanium oxide we made. The samples were prepared by spin casting the films on Si wafer. Because the three species of titanium oxide were treated at low temperatures, the film were amorphous as confirmed by X-ray diffraction (XRD). (Fig. 3.4). The typical XRD peaks of the anatase crystalline form appear only after sintering the spin-cast films at 450 °C for 2 hrs as shown., and the diffraction feature identical to the XRD patterns for the standard values of JCPDS No.21-1272(anatase TiO_2 crystal).

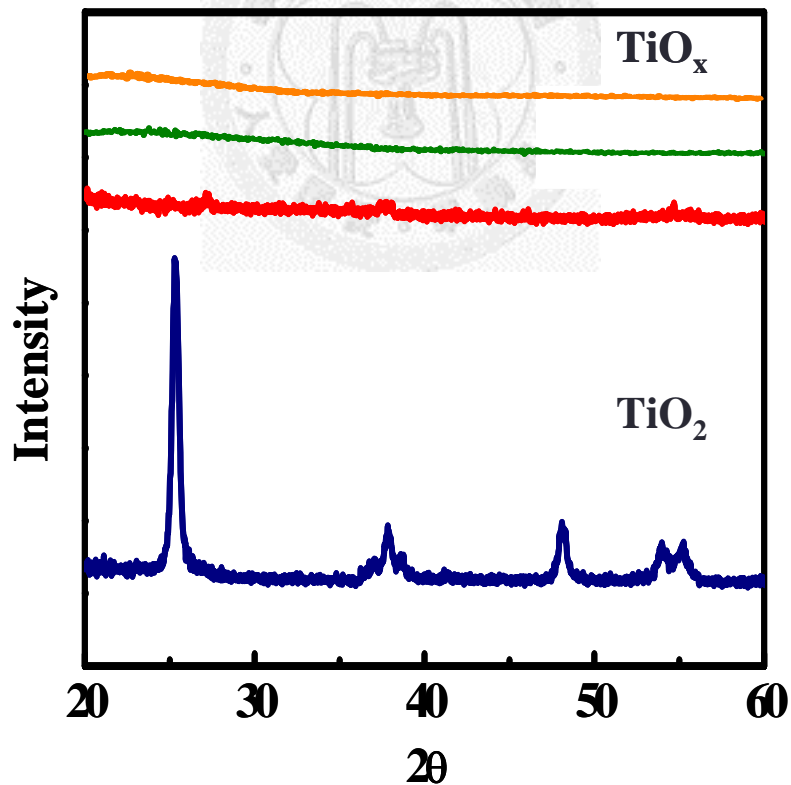


Fig. 3-4 X-ray diffraction pattern of titanium oxide, as synthesis(color orange to red, reaction time for 3hrs、6hrs and 9hrs, respectively.)

anneal at 450 °C(bottom)

3.4.2 X-ray photoelectron spectroscopy

To investigate the composition of synthesized TiO_x, high resolution XPS in accordance with Ti 2p and O 1s was shown in Fig. 3.5. Integrated peak area incorporate with sensitivity factor (1.798 for Ti 2p and O 1s 0.711) was applied for composition calculation. The O/Ti ratio was found to increase with respect to prolonging hydrolysis duration. The O/Ti ratio could be controlled in the regime from 1.5 to 1.9. (shown as Table 3.1) The lateral representation for TiO_x with different composition were demonstrated as low, medium and high respected to the hydrolysis duration.

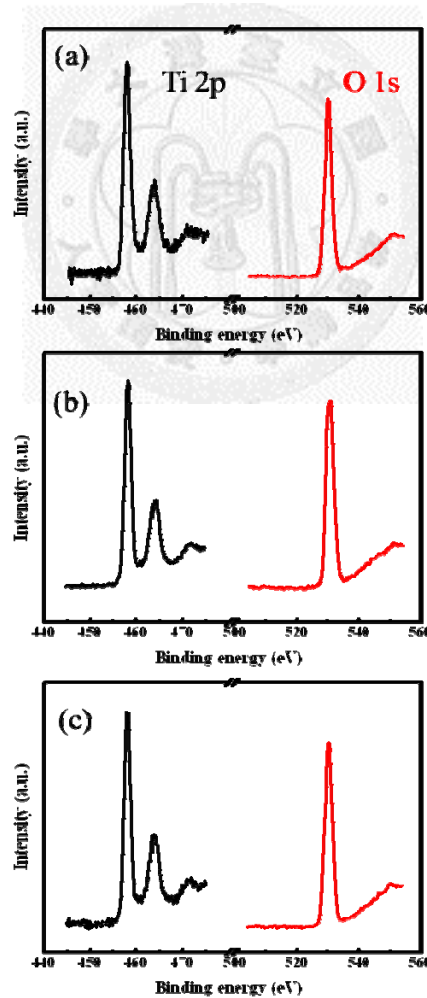


Fig. 3-5 XPS quantification of atomic composition for reaction (a)3hrs 、(b)6hrs 、

(c)9hrs

Table 3-1 O/Ti atomic ratio for different reaction time.

Low(3hrs)	Medium(6hrs)	High(9hrs)
1.51	1.68	1.91

Calculated O/Ti ratio indicated the synthesized TiO_x from sol-gel approach is chemically non-stoichiometric compound. Deconvolution of Ti 2p spectra for TiO_x with different O/Ti ratio was shown in Fig. 3.6. The TiO_{2-x} component was found to decrease with prolonging hydrolysis duration. Binding energy shift from 457.6 eV to 458.1 eV was also observed with respect with duration. More interestingly, color of synthesized TiO_x gel was found to turn from light yellow to deep orange with prolonging duration as indicated in in Fig. 3.6. Since color of transition metal compound is highly affected by coordination number, color change from colorless to yellow of titanium complex was observed due to coordination change from 4 to 5.^[17] Recall the TEM image in Fig. 3.7, particle size growth was highly affected by hydrolysis duration. With the aspect of crystal growth, dangling bond is commonly appeared in small size nanostructure, number of such dangling bond trend to truncate with enlarge size of nanocrystal (i.e. through maximize the coordination number of central atom). Regarding the above evidences and compare the binding energy of anatase phase TiO_2 (459.1 eV)^[11], the binding energy shift toward higher binding energy region could attribute to the progressing enhancement of coordination number during hydrolysis.

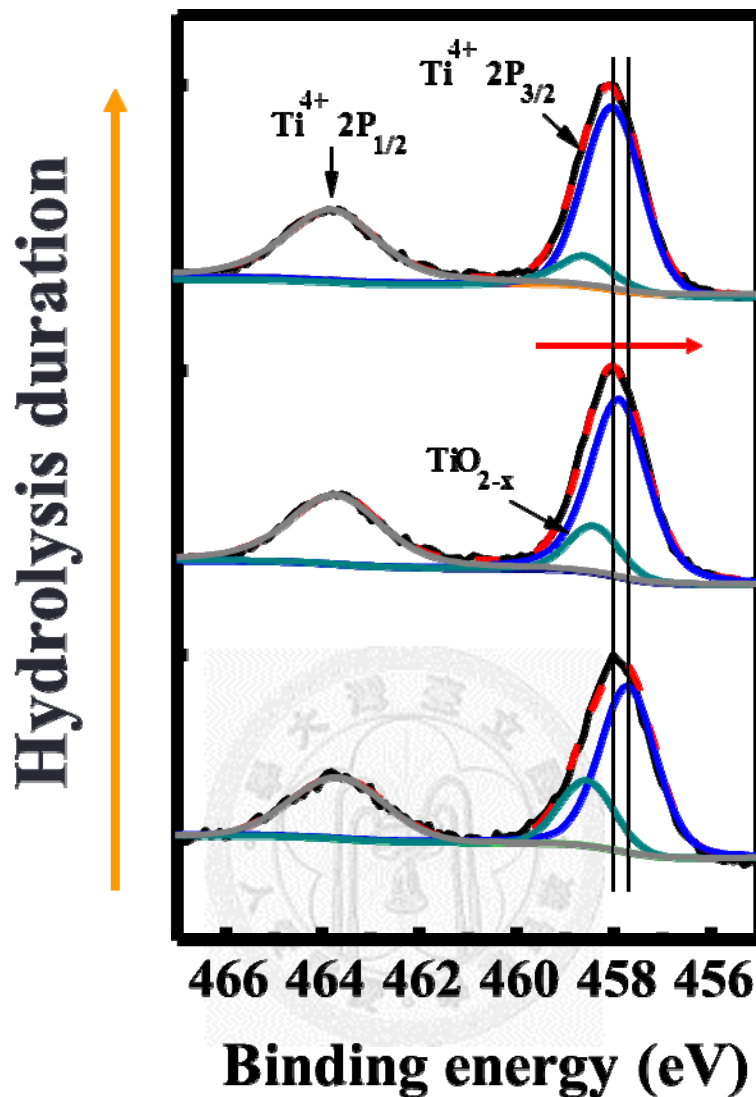


Fig. 3-6 Ti 2p XPS spectra of titanium oxide with different reaction time after deconvolution. Reaction for (a) 3hrs (b) 6hrs (c) 9hrs

3.4.3 Transmission electron microscopy

As the reaction time become longer, the color of titanium oxide become more deep (it's from light yellow to deep oxblood red). From TEM image, the particle size of titanium oxide increase with the reaction time (Fig. 3.7). The diameter w is about ~10nm for the lowest O/Ti ratio and ~20 nm for the highest O/Ti ratio.

We could explain that, the more reaction time we made the more alcoxolation or condensation reaction occur, so the radical bond to the others and expand to a more larger particle in 3-dimension.

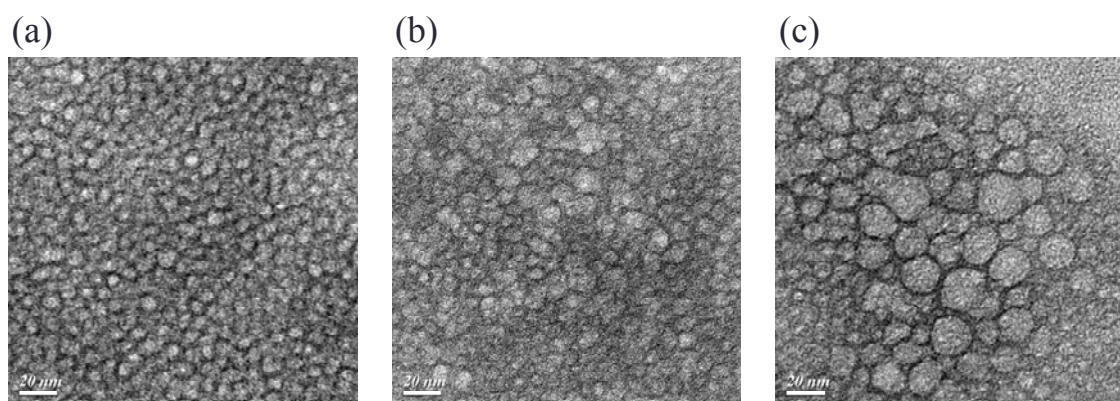
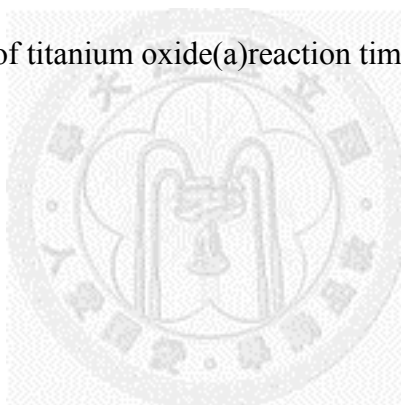


Fig. 3-7 TEM image of titanium oxide(a)reaction time = 3hrs (b)6hrs (c) 9hrs



3.5 Determine the Energy Gap and Conduction Band Level of Titanium Oxide

3.5.1 UV-Visible spectroscopy

Deposited titanium oxide film of different O/Ti ratio solution on glass by spinning and measure the absorbance spectrum. Fig. 3.8 is the absorbance spectrum of different species, the IR and UV range is not obvious different, but 350nm-500nm is quite different. From the spectrum, the absorption of titanium oxide with high O/Ti is more than others.

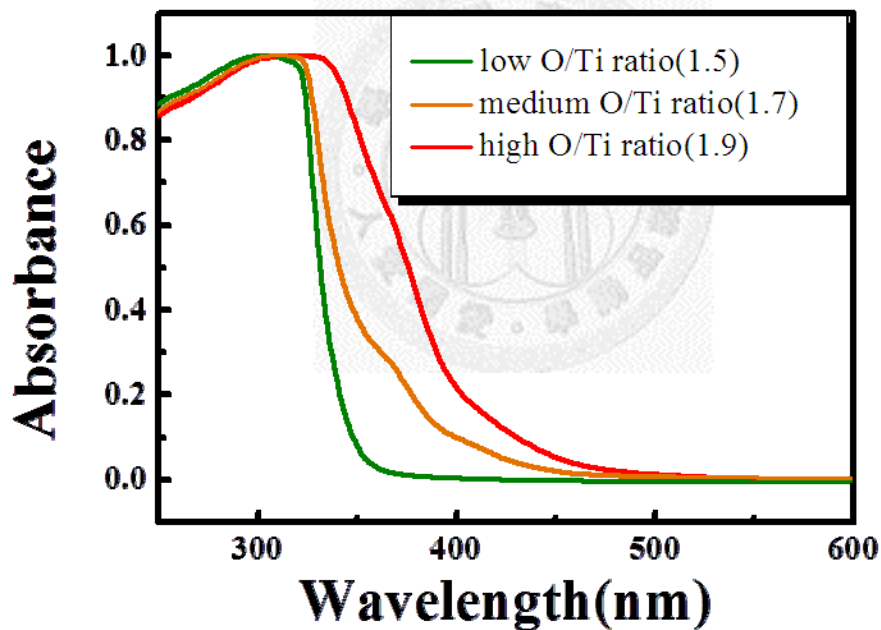


Fig. 3-8 Absorbance spectrum for different O/Ti ratio.

The band gap of material can be determined the Tauc plot^[12]. Tauc's plot shows the quantity $h\nu$ (the energy of the light) on the abscissa and the quantity $(\alpha h\nu)^r$ on the ordinate, where α is the absorption coefficient of the material. The value of the exponent

r denotes the nature of the transition; for example, $r = \frac{1}{2}$ for indirect transitions

$$(\alpha h\nu)^{\frac{1}{2}} = B^{\frac{1}{2}} (h\nu - E_g) \quad (3.1)$$

The resulting plot has a distinct linear regime which denotes the onset of absorption. According to equation (3.1), the interception of x-axis represent for the band gap of the material. Figure 4.8 show the result, the energy band is 3.75eV、3.62eV、3.25eV for three different O/Ti ratio, respectively. The energy gap is about 3.2ev for TiO₂ nanoparticle, so when the reaction time more longer, the O/Ti ratio approach to 2:1 and the energy gap approach to TiO₂.

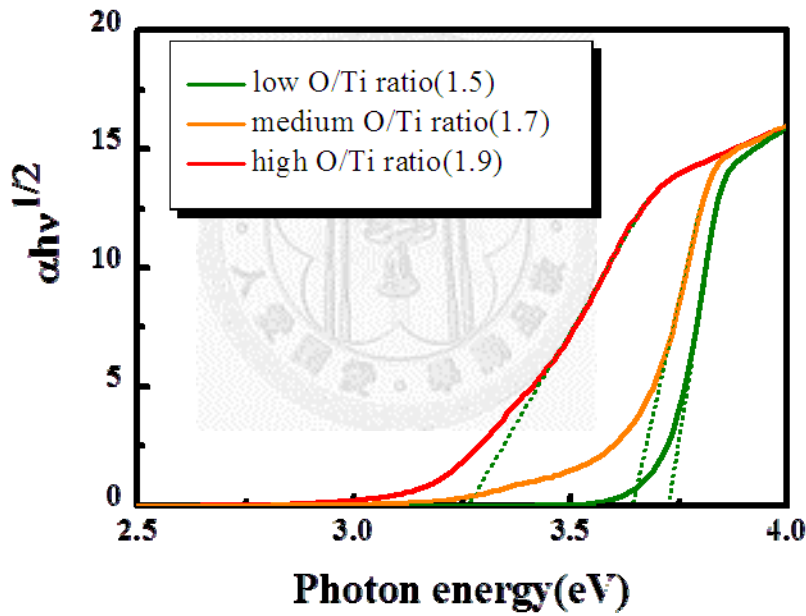


Fig. 3-9 Tauc plot of titanium oxide with different O/Ti ratio

3.5.2 Cyclic voltammetry measurement

From the Tauc plot, we know the band gap is quite different from the O/Ti ratio. If a material that can be used as an electron transport layer, the level of conduction band preferably lower than the LUMO of the electron acceptor, here, PCBM.

Cyclic voltammetry is a useful tool to determine the band position of an unknown material. By utilizing a known material (Ferrocene) as a reference, we can get the band position of the unknown material which relative to the band position of reference. By equation (4.2), we can calculate the band position of material relative to vacuum level.

$$Ec = [-e(E_{onset(vs. Ag / AgCl)} - E_{(Fc / Fc^{+} vs. Ag / AgCl)})] - 4.8 eV \quad (3.2)$$

From data of cyclic voltammetry, the onset position for low ratio to high is -1.22V 、 -1.17V 、 -0.94V, respectively. By equation (3.2), we calculate the band position relative to vacuum is 3.92eV 、 4.11eV 、 4.32eV. Then, combine to the band gap (Fig. 3.9), we can get the level of conduction and valance band. Fig. 3.14 shows the band diagram of the titanium oxide of different O/Ti ratio. By data of absorption and cyclic voltammetry, we also determine the band position of TiO₂ nanoparticle.(Fig. 3.13)

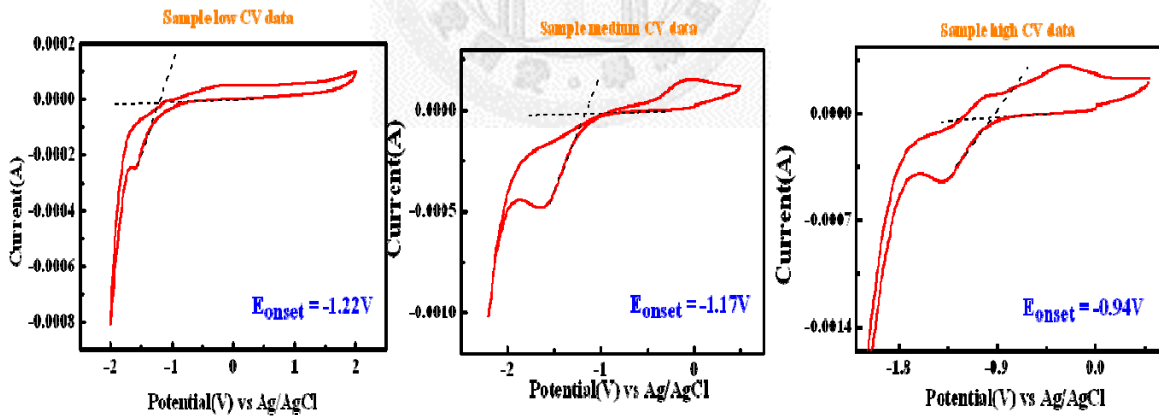


Fig. 3-10 Cyclic voltammograms of titanium oxide with different O/Ti ratio
low(left), medium(middle), high(right).

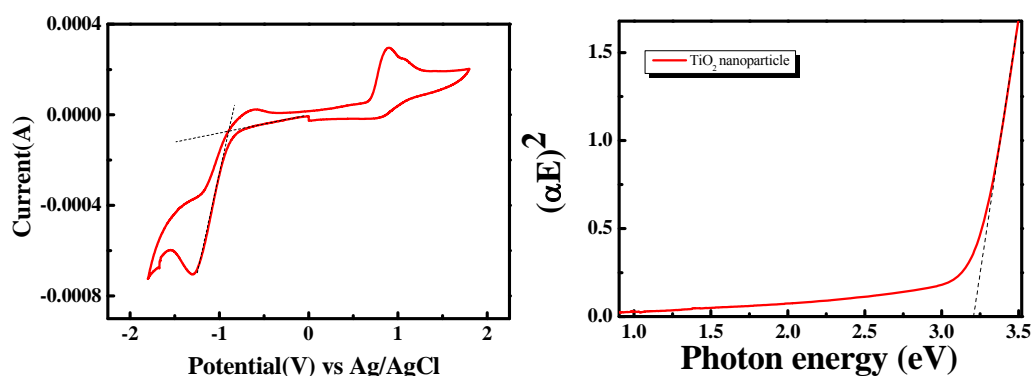


Fig. 3-11 Cyclic voltammograms and Tauc plot of TiO₂

Table 3-2 Summarized of the conduction and valence band level

	$E_{\text{Fc/Fc}^+}$ vs Ag/AgCl (V)	E_c (eV)	E_g (eV)	E_v (eV)
Low	0.48	-3.92	3.75	-7.73
Medium	0.48	-4.11	3.62	-7.7
High	0.48	-4.32	3.28	-7.6
TiO ₂	0.48	-4.37	3.21	-7.58

Fig. 3.12 shows the band diagram with different O/Ti ratio. When increase the O/Ti ratio, the band gap become smaller and the position of conduction and valance band change simultaneously. The position of conduction band decrease from 3.92eV to 4.32eV when 4.37eV for TiO₂ nanoparticle. The position of valance band increase from 7.73eV to 7.60eV when 7.58eV for TiO₂ nanoparticle. In a nutshell, more reaction time we made, more O/Ti ratio we get and the band diagram is more like to TiO₂ nanoparticle.

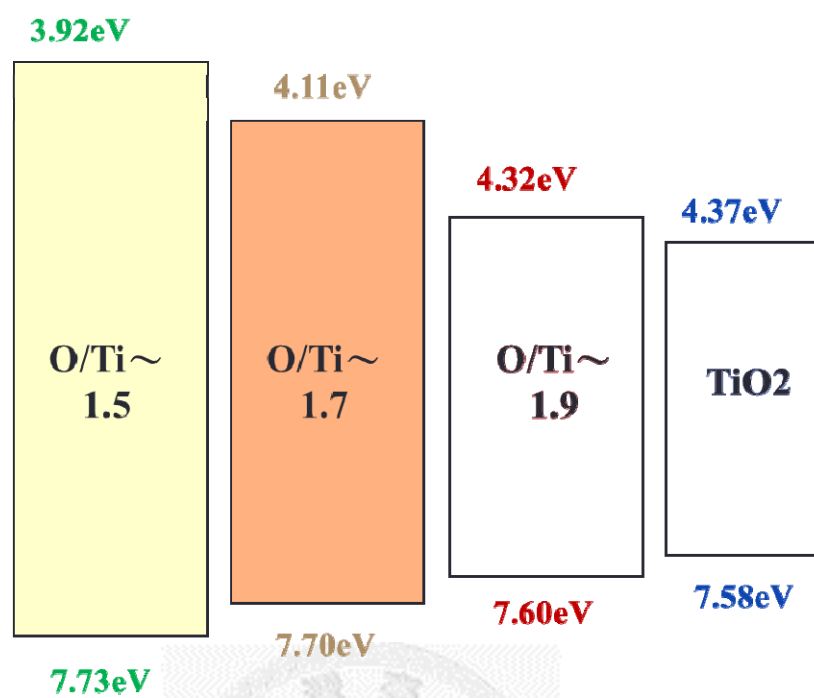


Fig. 3-12 band diagram of titanium oxide with different O/Ti ratio.

3.6 Reference

- [1] C.F Base and R. E. Messmer, The hydrolysis of Cations (Wiley, N.Y., 1976).
- [2] D. C. Bradley, R. c. Mehrotra, and D. P. Gaur, Metal Alkoxides (Academic Press, N. Y., 1978).
- [3] J. Livage, M. Henry, and C. Sanchez, “Sol-Gel Chemistry of Transition Metal Oxides“ in Progress in *Solid State Chemistry*, 18 (1988) 259-342.
- [4] C. Sanchez, J. Livage, M. Henry, and F. Babonneau, *J. Non-Cryst. Solid*, 100 (1988) 65-76.
- [5] W. Geffcken and E. Berger, Deutsches Reichspatent 736411, assigned to Jenaer Glaswerke Schott & Gen., Jena.
- [6] H. Schroeder in *Physics of the Thin Films*, ed. G. Hass, **5** 87-141.
- [7] J. Livage and K. Lemerle, Ann. Rev. Matter. DSci., **12** 103-122.
- [8] J. Livage in *Better Ceramics Through Chemistry*, eds. C.J. Brinker, D.E. Clark, and D.R. p.125.
- [9] M. Guglielmi and A. Maddalena, *J. Mat. Sci. Lett.*, **4** (1985) 123.
- [10] W.W. Davison, S.G. Shyu, R.D. Roseman, and R.C. Buchanan in *Better Ceramics Through Chemistry III*, p797.
- [11] Atashbar, M. Z.; Sun, H. T.; Gong, B.; Wlodarski, W.; Lamb, R., XPS study of Nb-doped oxygen sensing TiO₂ thin films prepared by sol-gel method. *Thin Solid Films* **1998**, 326 (1–2), 238-244.
- [12] Tauc, J., Optical properties and electronic structure of amorphous Ge and Si. *Materials Research Bulletin* **1968**, 3 (1), 37-46.
- [13] Kim, J. Y.; Kim, S. H.; Lee, H. H.; Lee, K.; Ma, W.; Gong, X.; Heeger, A. J., New Architecture for High-Efficiency Polymer Photovoltaic Cells Using

- Solution-Based Titanium Oxide as an Optical Spacer. *Advanced Materials* **2006**, *18* (5), 572-576.
- [14] Lee, K., J. Y. Kim, et al. (2007). "Air-Stable Polymer Electronic Devices." *Advanced Materials* **19**(18): 2445-2449.
- [15] Kim, J. Y., K. Lee, et al. (2007). "Efficient Tandem Polymer Solar Cells Fabricated by All-Solution Processing." *Science* **317**(5835): 222-225.
- [16] Lee, K., J. Y. Kim, et al. (2009). Titanium Oxide Films as Multifunctional Components in Bulk Heterojunction "Plastic" Solar Cells. *Organic Photovoltaics*, Wiley-VCH Verlag GmbH & Co. KGaA: 261-280.
- [17] Adachi, M.; Murata, Y.; Takao, J.; Jiu, J.; Sakamoto, M.; Wang, F., Highly Efficient Dye-Sensitized Solar Cells with a Titania Thin-Film Electrode Composed of a Network Structure of Single-Crystal-like TiO₂ Nanowires Made by the "Oriented Attachment" Mechanism. *Journal of the American Chemical Society* **2004**, *126* (45), 14943-14949.

◦

Chapter 4 The Performance of Device with Different Titanium Oxide as Electron Transport Layer

4.1 Fabrication of Polymer Solar Cell with Titanium Oxide

The photovoltaic device was fabricated as following procedures, ITO substrates were etched and clean with acetone 、methanol 、DI water : Hydrogen peroxide : Ammonia (volume ratio, 5:1:1) and isopropanol then dried with nitrogen flush.

Device structure shows in Fig. 4.1. Substrates were treated with oxygen plasma for 5 minutes after that the work function of ITO will increase and the surface become hydrophilic. PEDOT:PSS as hole transport layer was spin-cast on the ITO substrate(5000rpm, 50s), it can also smooth the ITO surface. The photoactive layer was deposited on the top of the PEDOT:PSS layer by spin coating using a 10:8 weight ratio blend consisting of P3HT and PCBM dissolved in chlorobenzene. The titanium oxide as electron transport layer was spin-cast (3000rpm ,30s) on the top of the photoactive layer then annealed at 80°C in air(10minutes) to remove the residual solvent. The aluminum electrode was deposited by thermal evaporation in a vacuum at a pressure about 5×10^{-6} Torr. Before the measurement, the device will anneal 150°C to crystallize the photoactive layer then get a better performance.

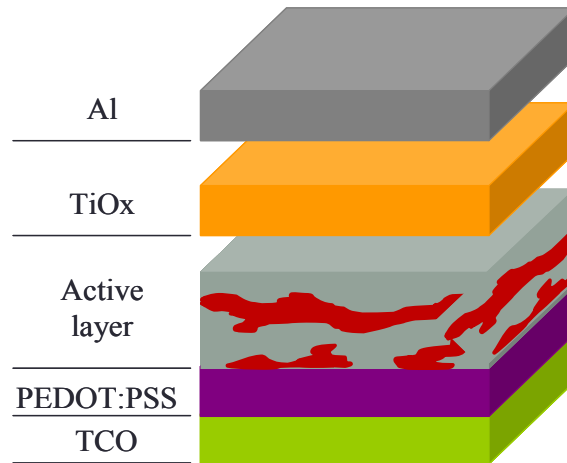


Fig. 4-1 Structure of the device with TiO_x

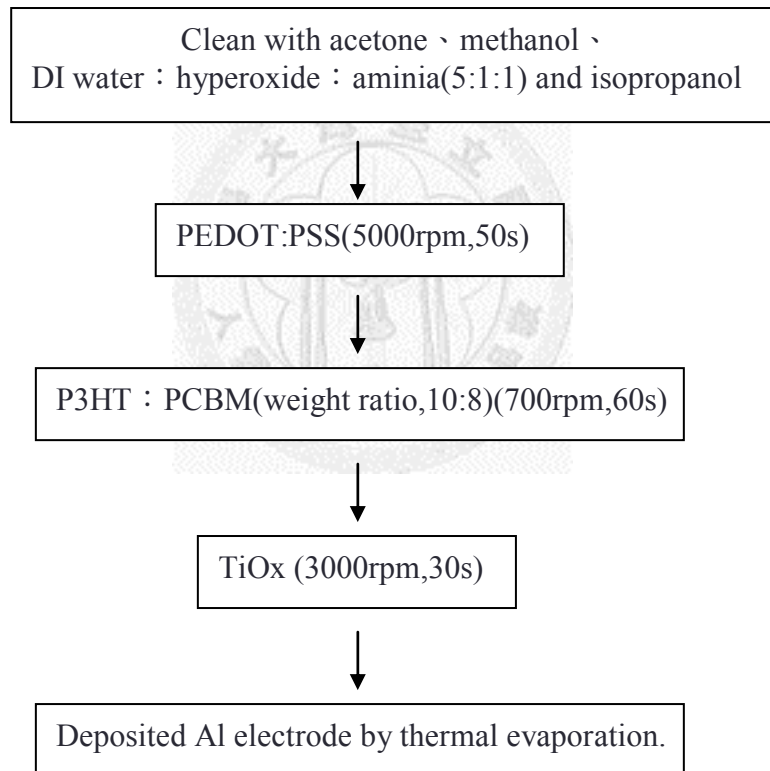


Fig. 4-2 the flow chart shows the procedure for preparing device.

The band diagram of the entire device depict in Figure 5.3. The n-type material which facilitates electron transfer from the LUMO of the acceptor to the conduction band of the metal oxide. The conduction band level of TiO_x is lower than the LUMO of PCBM, so the photoinduced electrons in active layer will transfer to TiO_x . And the valance band level of TiO_x is lower than the HOMO of PCBM so it can also block the hole carries and reduce the recombination.

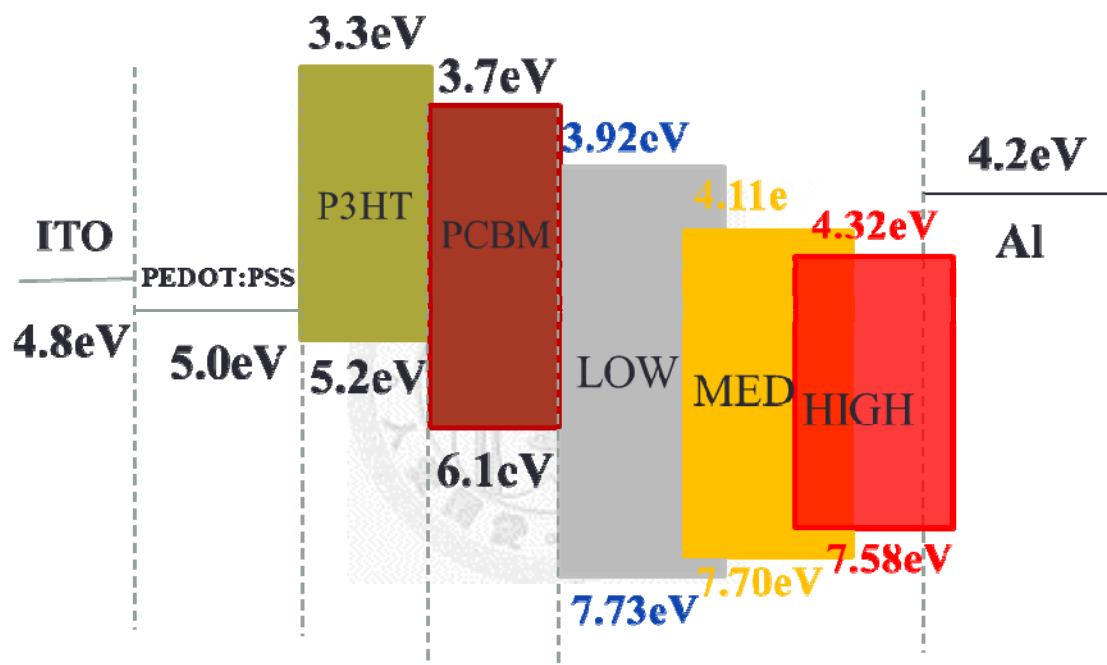


Fig. 4-3 Band diagram of the device

4.2 Device Performance with TiO_x Dispensed in Different Solvent

Because the concentration of original TiO_x solution is too high to spin on the top of active layer, it will be difficult to form a uniform film so we will dilute the solution. We use alcohols (2-methoxyethanol) as our solvent during synthesis process, in order to get a miscible solution we choose several alcohols as our dilute solvent.

We use butanol, pentanol, hexanol as our dilute solvent, volume ratio of 1:100 to dilute the original solution. Fig. 4.4 shows the device performance using different dilute solvent. The short-circuit current density (J_{sc}), open-circuit voltage (V_{oc}), fill factor (FF), and power conversion efficiency values for device are summarized in table 4.1. The insertion of TiO_x as an electron transport layer between active layer and Al electrode result in a substantial increase V_{oc} and J_{sc} , leading to an enhancement in power conversion efficiency (4.11%) for dilute in butanol. Pentanol also enhance the performance but not better than butanol as the dilute solvent, but hexanol not only decrease efficiency but also reduce the overall performance.

Table 4-1 Summaries of the device performance of conventional polymer solar cells using TiO_x as electron transport layer dilute in different solvent.

	$V_{oc}(V)$	$J_{sc}(mA/cm^2)$	FF(%)	η (%)
Conventional	0.57	9.40	57.2	3.43
Butanol	0.64	9.69	63.1	4.11
Pentanol	0.59	9.46	58.2	3.51
Hexanol	0.57	8.87	54.3	2.97

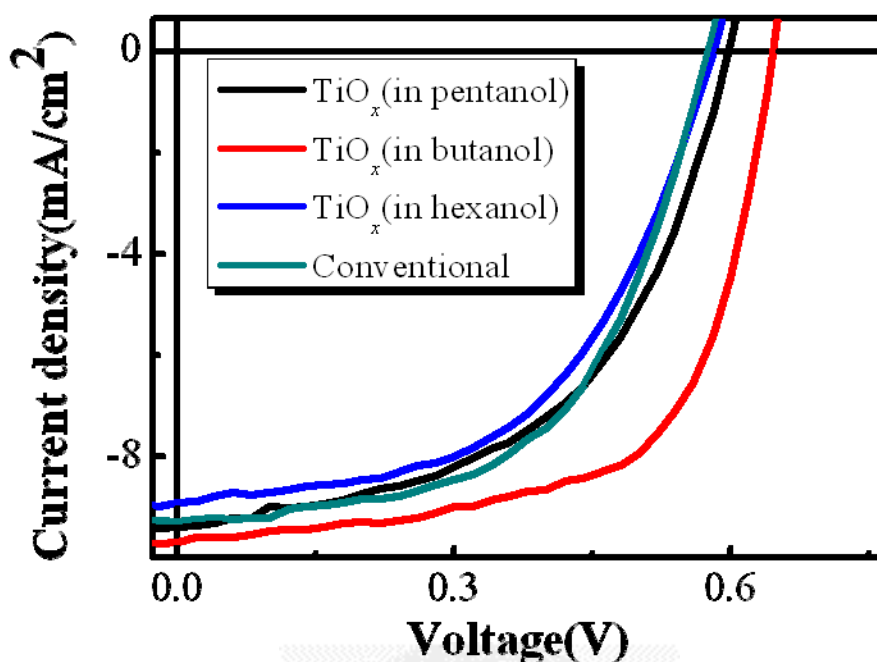


Fig. 4-4 Current-voltage characteristics of the polymer solar cells consisting of TiO_x as an electron transport layer. dilute in different solvent.

Generally speaking, the nanomorphology is important for device performance. Fig. 4.5 shows the morphology and phase image of the active layer covered by TiO_x dilute in different solvent. From AFM image, the morphology is not obviously different from solvent but the phase image is quite different. the roughness values is 3.78 nm(in butanol) 、4.96 nm(in pentanol) and 5.56 nm(in hexanol), respectively.

Fig. 4.6(a) shows the phase image of the active layer, the contrast is very strong because of the phase separation of P3HT and PCBM. When TiO_x spin on the active layer, the phase image is different from P3HT:PCBM. Fig. 4.6(b)-(d) show the phase image of TiO_x spin on the active layer. The butanol as solvent result in a uniform thin film in the active layer when pentanol is a semi-continuous. However, hexanol as dilute solvent cause a non-continuous film so reduce the device performance. Based on these

results, butanol is a good dilute solvent that can form a uniform, dense film on active layer. Because of this, it reflects the reason of butanol as a solvent can have better performance. In the follow-up study, we select butanol as a solvent to mix with our original solution.

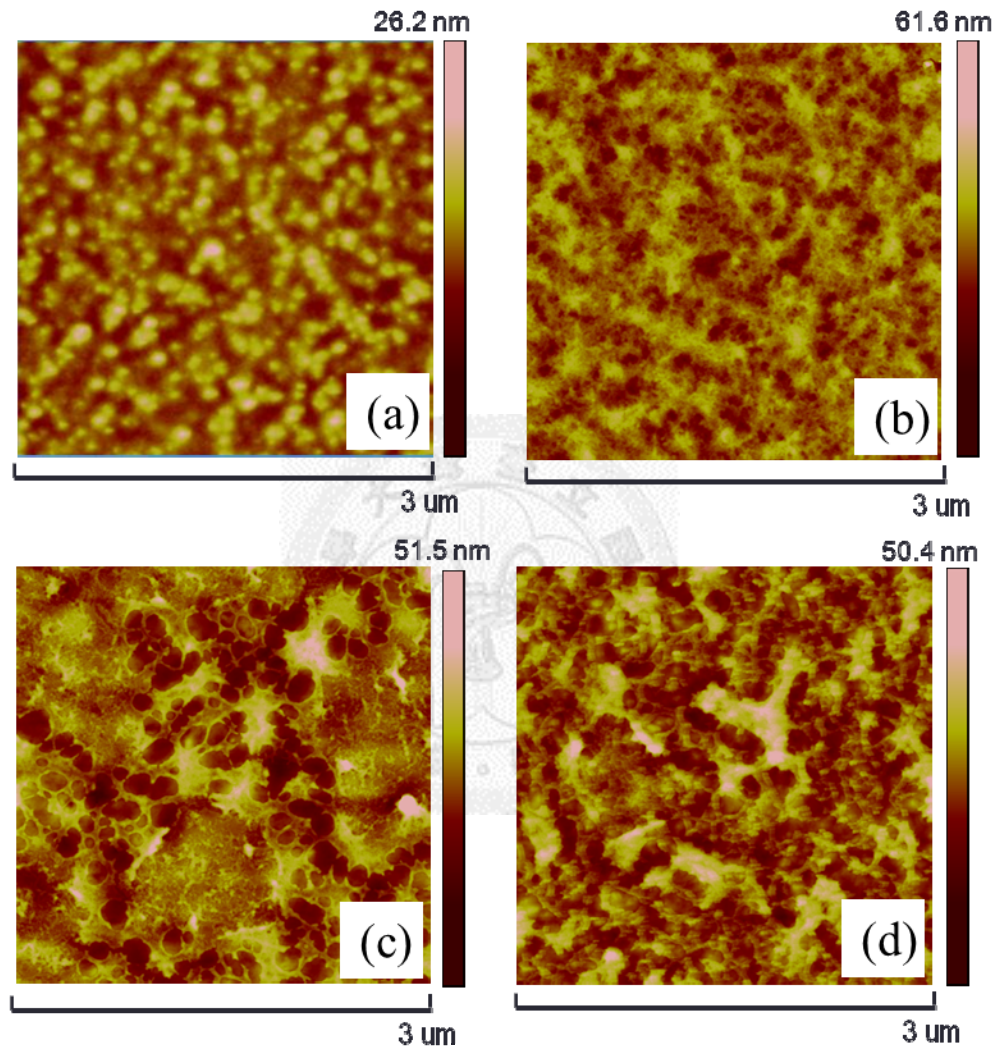


Fig. 4-5 the morphology of titanium oxide dilute in different solvent.

(a)original active layer(b)cover by titanium oxide(dilute in butanol) (c) cover by titanium oxide(dilute in pentanol) (d) cover by titanium oxide(dilute in hexanol)

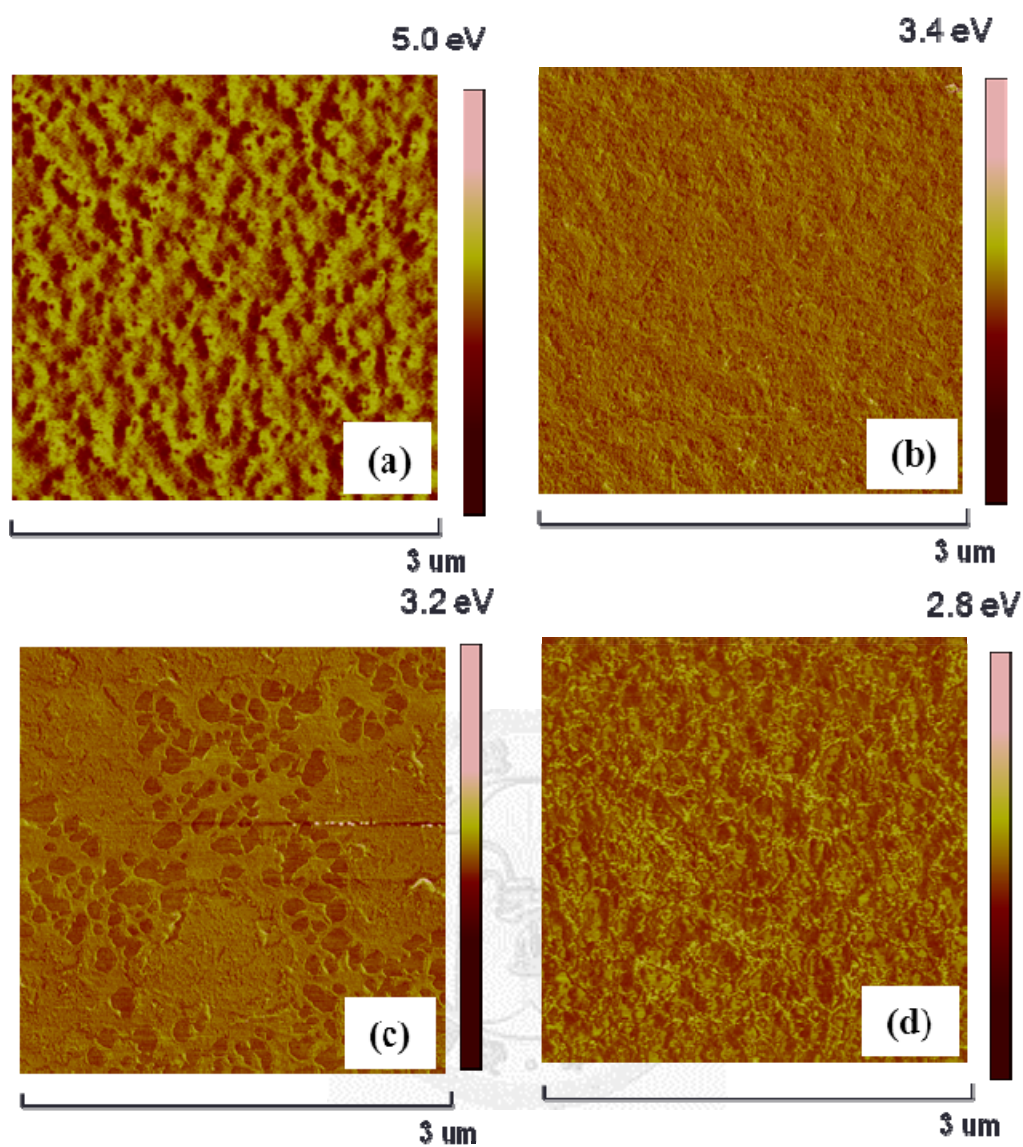


Fig. 4-6 the phase image of titanium oxide dilute in different solvent.

(a)original active layer(b)cover by titanium oxide(dilute in butanol) (c) cover by titanium oxide(dilute in pentanol) (d) cover by titanium oxide(dilute in hexanol)

4.3 Device Performance with Different O/Ti Ratio

4.3.1 Device performance

From Fig. 4.3, titanium oxide with different O/Ti ratio can be used as the electron transport layer because of their conduction band level is lower than the LUMO of PCBM, so we spin the different titanium oxide on top of active layer and observe the effect of different conduction band level on our devices. Fig. 4.7 shows the device performance using different O/Ti ratio. The short-circuit current density (J_{sc}), open-circuit voltage (V_{oc}), fill factor (FF), and power conversion efficiency values for device are summarized in table 4.2. From table 4.2, we can see when increase O/Ti ratio, the performance is quite different. The devices with low O/Ti ratio have the best performance and the value of J_{sc} , V_{oc} , FF, is higher than device without TiO_x . The device with medium O/Ti ratio enhanced the device performance slightly. However, the device with high O/Ti ratio degraded overall performance. Fig. 4.8 shows the EQE spectrum of device fabricated with and without the TiO_x . For the device with the TiO_x layer, the result demonstrate a substantial enhancement in the EQE over the spectrum that respond to the enhancement of J_{sc} .

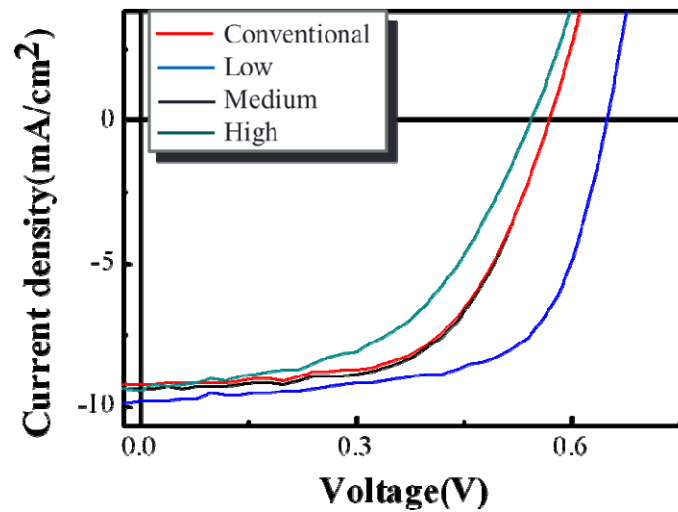


Fig. 4-7 J-V curve of the device with different TiO_x

Table 4-2 Summaries of the device performance of different O/Ti ratio.

	Voc(V)	Jsc(mA/cm ²)	FF(%)	η (%)
Conventional	0.57	9.19	57.6	3.23
Low	0.63	9.83	66.7	4.11
Medium	0.57	9.38	58.1	3.28
High	0.51	9.21	54.6	2.63

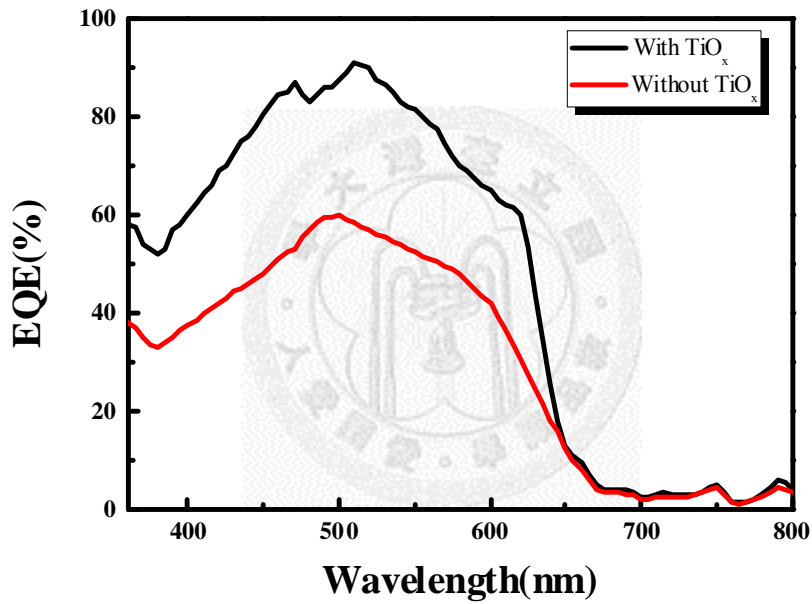


Fig. 4-8 External quantum efficiency spectra for devices with and without the TiO_x

We clearly see an improvement in Voc, Jsc, and fill factor (FF) for the devices with titanium oxide with low O/Ti ratio, resulting in efficient device performances. The Voc increases from 0.57 V (for the device with no interlayer) to 0.63 V and the FF improves dramatically up to 66.64%. This yields power conversion efficiency (PCE) of 4.11%. The device with medium O/Ti ratio also improve the performance (Voc=0.57, Jsc=9.38mA/cm², FF=58.12% PCE=3.28%), but its effect is less than the device with

low O/Ti ratio. ($V_{oc}=0.63$, $J_{sc}=9.83 \text{ mA/cm}^2$, $FF=66.64\%$ $PCE=4.11\%$). However, the device with high O/Ti ratio not only did not improve the device but cause decay ($V_{oc}=0.51$, $J_{sc}=9.21 \text{ mA/cm}^2$, $FF=54.59\%$, $PCE=2.63\%$).

The morphology is important for device performance, so the various device performance also may be caused by the different of morphology. Fig. 4.9 shows the AFM image of the devices with different O/Ti ratio. From these images, these three species don't have obvious different, all these species have the similar morphology. Therefore, the morphology will not be the main reason for the different device performance that may cause by other factor.

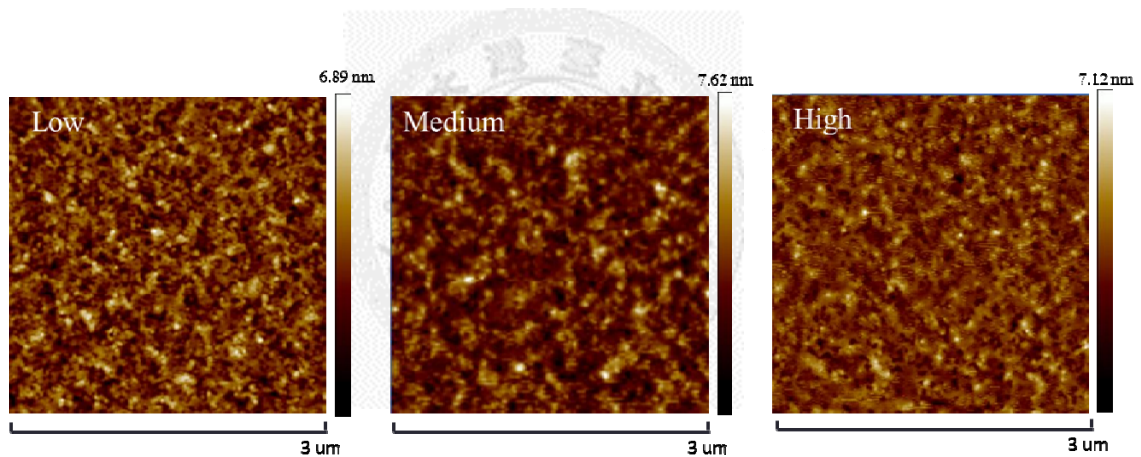


Fig. 4-9 AFM image of titanium oxide with different O/Ti ratio (a)low O/Ti ratio(b)medium O/Ti ratio(c)high O/Ti ratio

4.3.2 The effect of band diagram

Because each device only the TiO_x layer was different, the characteristics of TiO_x must dominate the device performance. Review the above result, the most different characteristics for different O/Ti ratio is the band position.

Recall the band diagram of entire device (Fig. 4.3), the conduction level of TiO_x is

very different from O/Ti ratio. TiO_x provide an appropriate conduction band position is important for the electron transport from PCBM. Here, the conduction band position of different TiO_x is 3.92eV for low O/Ti ratio, 4.11eV for middle O/Ti ratio and 4.32eV for high O/Ti ratio. The conduction band position effect device performance is mentioned in the literature.^[7]

Y. Yang et al. modified the titanium oxide by doping Cs and the device performance is greatly improvement. They explained that the improvement of device performance is from the conduction band position changing. The conduction band level of TiO_2 is 4.3 eV, which is slightly higher than the work function of 4.2 eV of the Al electrode. This results in unfavorable electron charge extraction from the active layer to the electrode. However, the modified titanium oxide formed a better Ohmic contact that is created by the decreased conduction band level of the titanium oxide layer (3.93 eV) such that the interfacial layer facilitates electron transport from the active layer to the cathode.

In this research, we change the conduction band level by modified the O/Ti ratio but not doping. However, the similar result we can observe. The conduction band level of high O/Ti ratio is 4.37 eV and the low O/Ti ratio is 3.92eV, these different may cause the similar effect, that the electron charge from active layer to electrode is unfavorable for high O/Ti ratio. Due to the fact, we believe the device performance be effected by the conduction band level, and cause the different device performance.

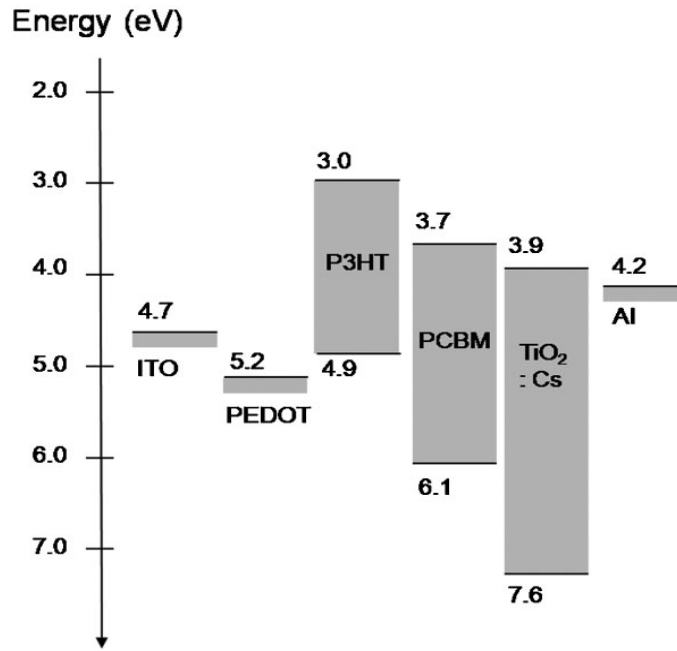


Fig. 4-10 Corresponding energy level diagram of a device based on a TiO₂:Cs. [7]

We have also noted that the open current voltage will change by introducing different titanium oxide. Table 4.3 summaries the open circuit voltage with different O/Ti ratio. In the literature, there are two explanations of the origin of open current voltage. If the device is non-ohmic contact, the Voc determined by the HOMO of electron donor and the LUMO of electron acceptor, the Voc increase with the different of LUMO_A and HOMO_D.^[8] If the device is ohmic contact, the Voc determined by the cathode and anode, the Voc increase with the different energy level of cathode and anode.^[9] According to the band diagram of our result, the model of non-ohmic is more suitable to describe this case. The TiO_x work as an interfacial layer between the cathode and active layer, in some degree it will modify the cathode. For low O/Ti ratio, the cathode be modified to a more negative energy level, that will result in a higher Voc. On the other hand, the high O/Ti ratio will shift the energy level of cathode to a more positive position, and reduce the Voc. t.

Table 4-3 Summaries the Voc of the device with different O/Ti ratio

	Voc (V)
Conventional	0.57
Low	0.63
Medium	0.57
High	0.51

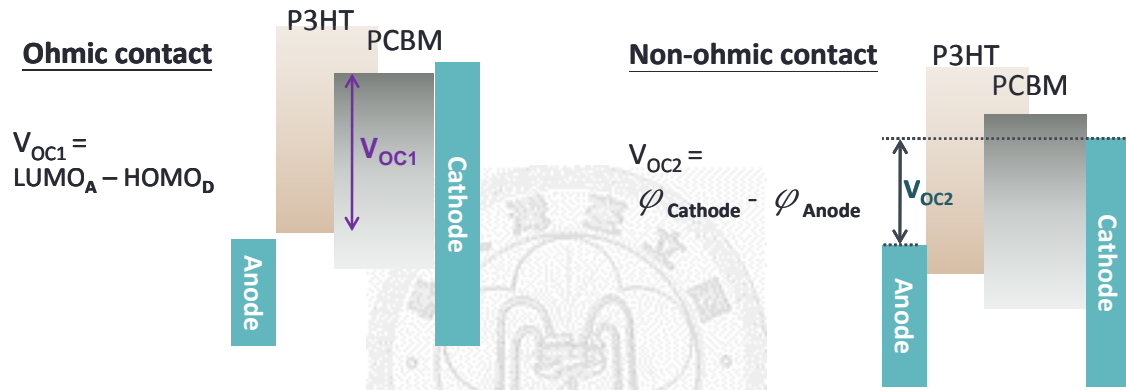


Fig. 4-11 Two explanations of the origin of open current voltage

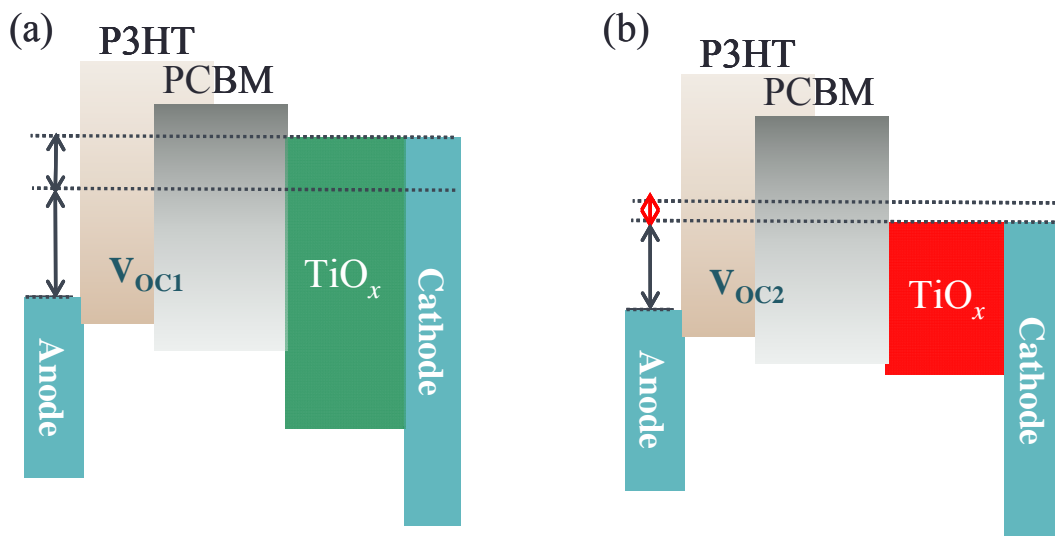


Fig. 4-12 the energy level of cathode.(a)modified by low O/Ti ratio, (b)modified by high O/Ti ratio.

4.3.3 The conductivity of different O/Ti ratio

The conductivity also plays an important role in OPVs. If we insert a material with high resistivity that will cause the decrease of J_{sc} . Usually, for hole transport layer, PEDOT is doped with PSS (poly(styrenesulfonate)) for improved conductivity.

Here, for the conductivity measurement, a 100nm-thick layer of Ag electrode was deposited onto a glass substrate. Then TiO_x layer was spin on the top of electrode. Then, the Ag electrode deposited on the TiO_x layer again by thermal evaporation. Fig. 4.12 shows the structure of the device.

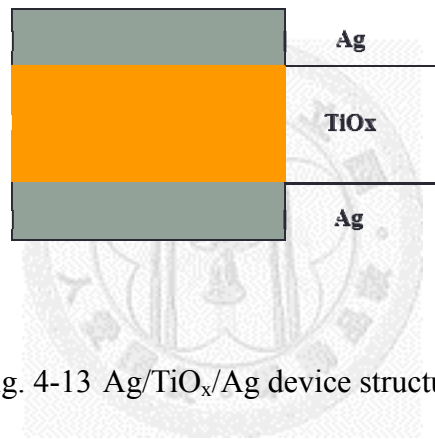


Fig. 4-13 Ag/ TiO_x /Ag device structure

Fig. 4.13 shows the I-V curve of the Ag- TiO_x -Ag device, the slopes of the curves increase as the lower O/Ti ratio. From the conductivity measurement, the conductivity increase when decrease the O/Ti ratio of titanium oxide, table 4-4 shows the measurement results. The similar results have been proposed in the literature^[2]. Fig. 4.14 shows the result of conductivity vs. O/Ti ratio. For nonstoichiometric thin films of TiO_x obtained by reactive sputtering. It demonstrates the existing correlation between the electrical resistivity and film composition. When the O/Ti ratio decrease, that is, for increasing deviation from the oxygen stoichiometry x , TiO_x thin films become more conducting. The close relationship between conductivity and x indicates that oxygen

nonstoichiometry is the source of electrons in the conduction band of titanium oxide thin films.

The conductivity measurement of Ag- TiO_x -Ag structure demonstrates higher O/Ti ratio decrease conductivity and increase the series resistivity in device.

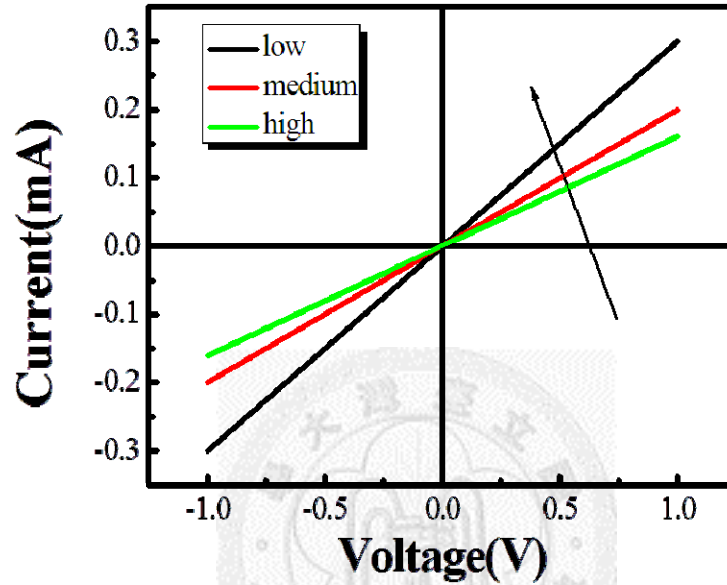


Fig. 4-14 I-V curve of the Ag- TiO_x -Ag device

Table 4-4 Electrical resistivity and conductivity of different titanium oxide

	Resistivity(Ω -cm)	Conductivity(Ω -cm) ⁻¹
Low	4974.51	2.11×10^{-4}
Medium	5847.58	1.71×10^{-4}
High	7167.72	1.39×10^{-4}

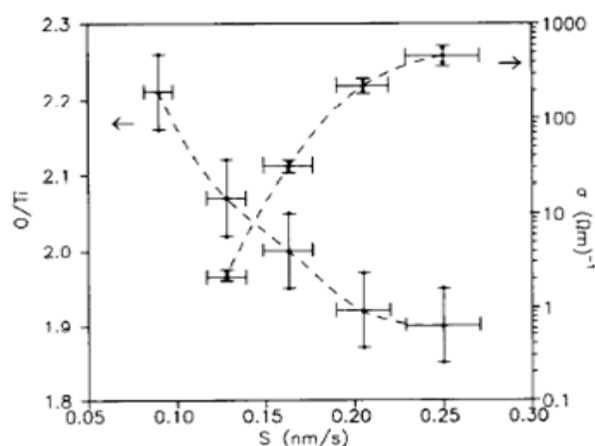


Fig. 4-15 Atomic ratio O/Ti of oxygen to titanium (left-hand scale) and electrical conductivity (right-hand scale) as a function of the growth rate of TiO_x films; lines drawn to guide the eye.^[2]

Based on the above, different conductivity and conduction band level caused by the O/Ti ratio. The titanium oxide with low O/Ti ratio used in OPVs can get a better device performance, because of the appropriate conduction band level facilitates electron transport from the active layer to the cathode, and also has a better conductivity.

4.3.4 Summary

By controlling the synthesis parameters, titanium oxide with different O/Ti ratio we get. Different O/Ti atomic ratio will effect the characteristics of titanium oxide. the band gap, conduction band level and the conductivity. These characteristics is related to the device performance, therefore different device performance we observed.

The titanium oxide with low O/Ti atomic ratio, it is the best one for electron transport layer in OPV because of its conduction level close to the LUMO of electron acceptor(PCBM) and the resistivity is also lower.

4.4 Air Stability of OPV with TiO_x

The diffusion of oxygen and water vapor into the photoactive layers is inevitable. Moreover, most semiconducting polymer materials degrade when exposed to humidity and/or oxygen, and photo-oxidation can be a serious problem.^[4,5]

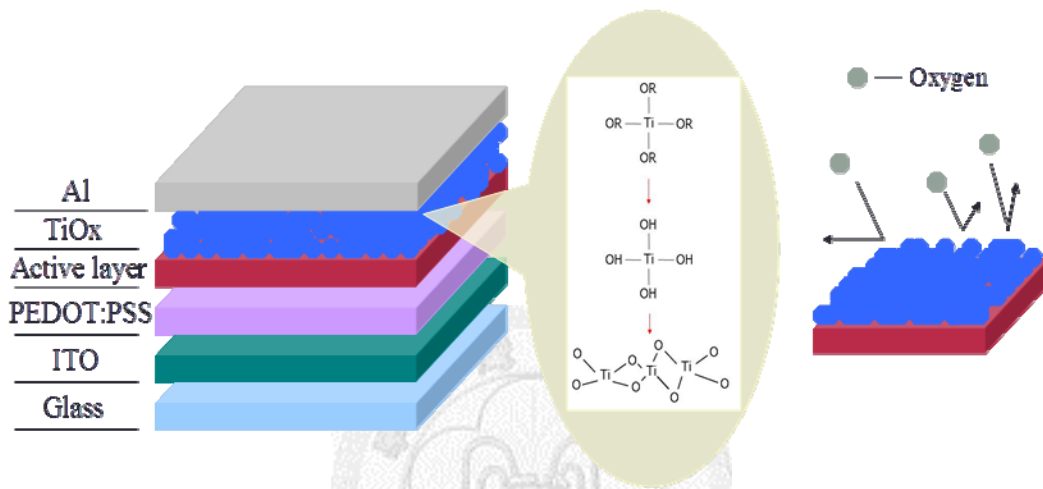


Fig. 4-16 The TiO_x layer acts as a shielding and scavenging layer which prevents the intrusion of oxygen and humidity into the electronically active polymers

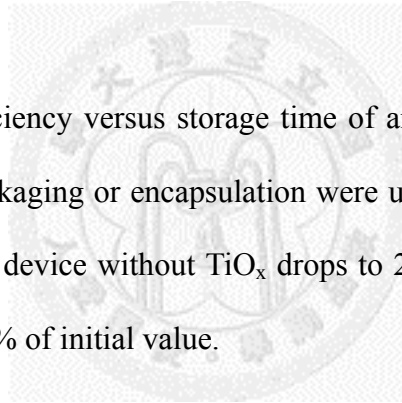
It has been proposed that inorganic oxides are quite stable to oxygen and moisture.^[6] By introducing a titanium oxide (TiO_x) layer between the active layer and the aluminum cathode in organic solar cell. The TiO_x interlayer promised the devices with excellent air stability and with enhanced performance.

The TiO_x layer acts as a shielding and scavenging layer which prevents the oxygen and humidity diffuse into the photoactive layer, therefore improving the lifetime of unpackaged devices exposed to air.

The TiO_x layer improves the lifetime of polymer-based solar cells. Fig. 4.16 compares the I-V curve The device without TiO_x shows typical photovoltaic response

with device performance; the short circuit current (J_{sc}) is $J_{sc} = 9.17 \text{ mA cm}^{-2}$, the open circuit voltage (V_{oc}) is $V_{oc} = 0.58 \text{ V}$, and the fill factor (FF) is $FF = 0.55$. These values correspond to a power conversion efficiency of $\eta = 3.36 \%$. When these devices were stored in the ambient air for 150 hours, a dramatic decrease in short circuit density was observed as the storage time increased, the PCE dropped from 3.36% to 0.61% and the V_{oc} also degraded from 0.58 V to 0.51 V. However, for the device with the TiO_x layer, the initial performance was comparable to those of the conventional devices without the TiO_x layer; $J_{sc} = 9.69 \text{ mA cm}^{-2}$, $V_{oc} = 0.64 \text{ V}$, $FF = 0.63$, yielding $\eta = 4.1 \%$ and even storage in air for 150 hours, the device performance still remains a good performance. ($\eta = 3.3 \%$) Note, these two type devices were fabricated by using the same procedure.

Fig. 4.17 shows the efficiency versus storage time of an OPV with and without the TiO_x layer (no external packaging or encapsulation were used). After storage in air for 150 hours, the efficiency of device without TiO_x drops to 20% of initial value, whereas the TiO_x device remains 85% of initial value.



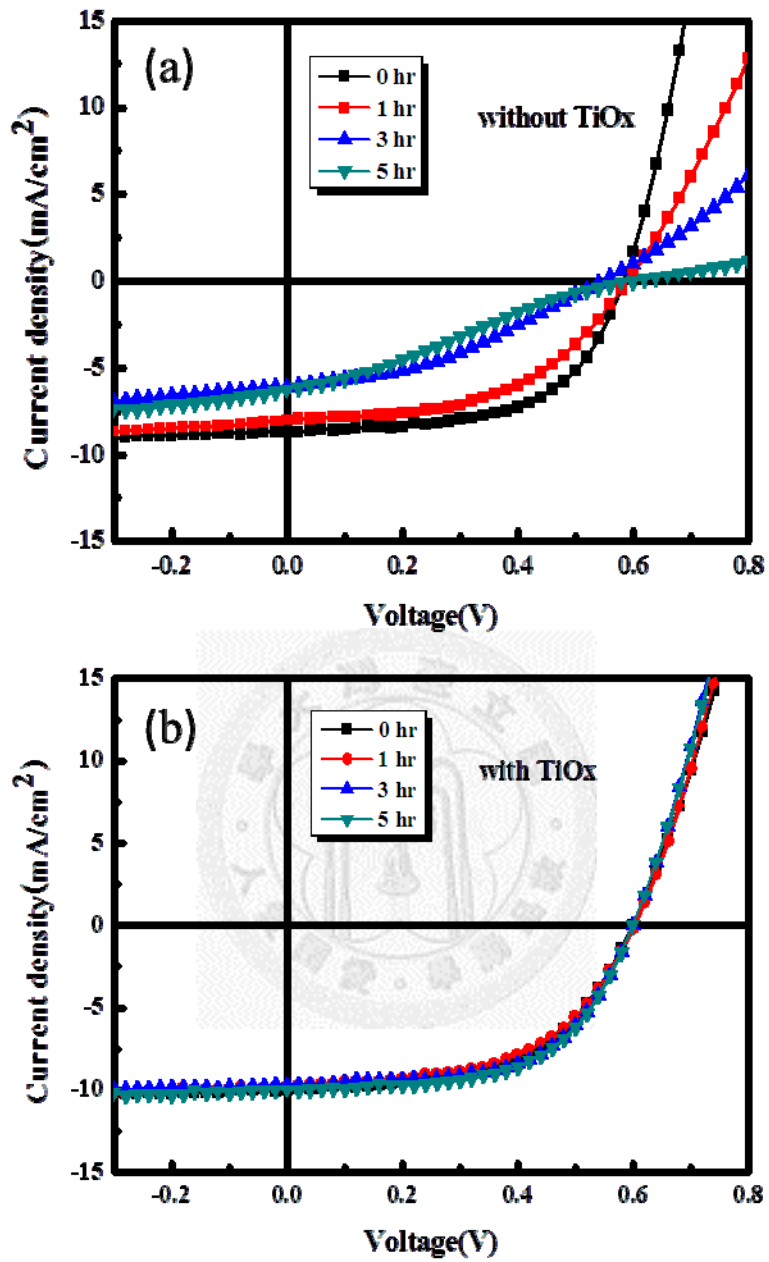


Fig. 4-17 Device performance as a function of storage time for polymer solar cells. The current density-voltage ($J-V$) characteristics of polymer solar cells with (a) and without the TiO_x layer (b)

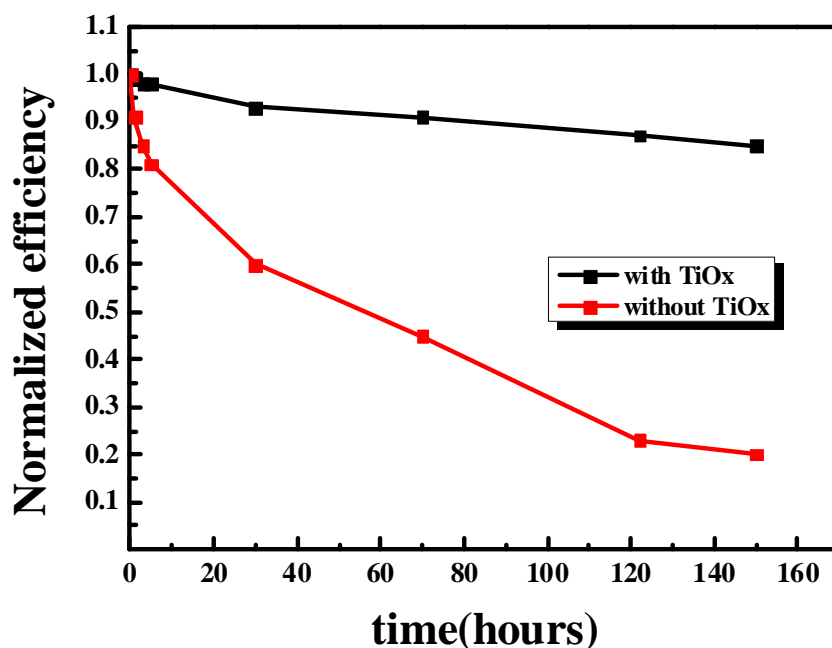


Fig. 4-18 Comparison of the power conversion efficiencies as a function of storage time for polymer solar cells with and without the TiO_x layer

In normal case, the device was used under illumination, therefore we also measure the air stability of device under illumination condition. Fig. 4.18 shows the device performance as a function of storage time for OPVs with and without the TiO_x layer measured after various storage time in the air under AM1.5 illumination from a solar simulator with an intensity of 100 mWcm^{-2} . Under illumination for two hours, the device with TiO_x still remain around ~95% of initial value in Voc, Jsc, FF and PCE, but the device without TiO_x decayed quickly in such condition, the Voc, Jsc, FF and PCE drop to around 80% of initial value.

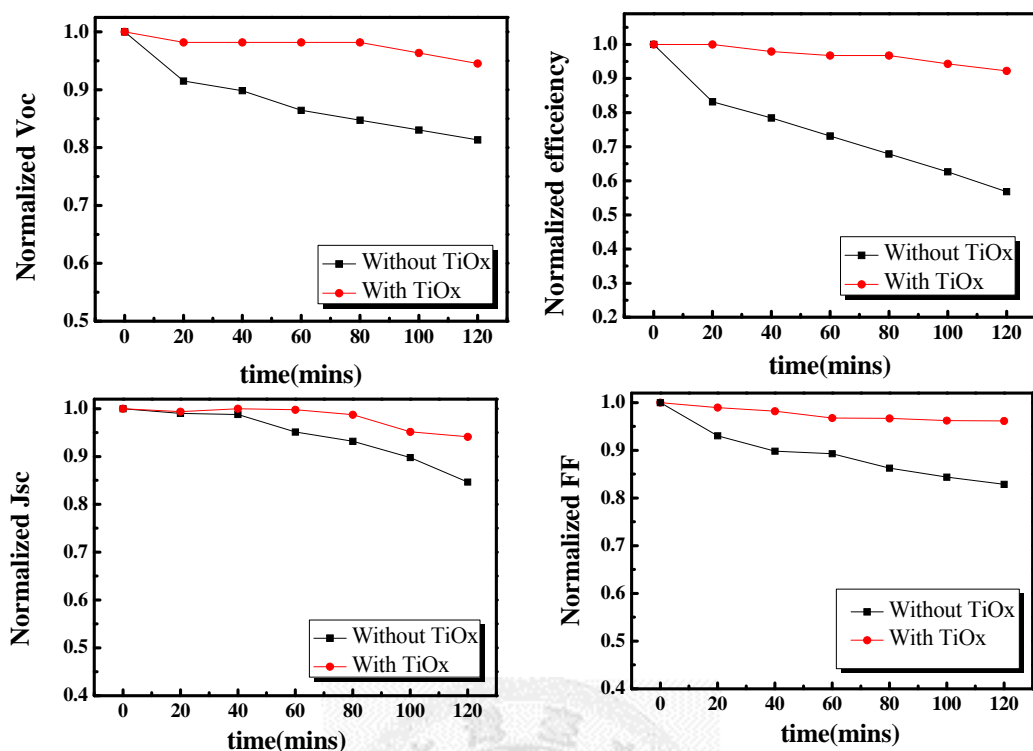


Fig. 4-19 the performance of device as a function of storage time for polymer solar cells with and without the TiO_x layer

Air stability of these two type devices (with and without TiO_x) exhibit a huge difference, AC impedance measurements were carried out to investigate the change in the performance of the device with TiO_x.

Fig. 4.19 shows the nyquist plots, the frequency range was from 20 Hz to 1 MHz, and the magnitude of the alternating signal was 5 mV. From the result of EIS, the R_p value gradually decrease from 1.1×10^4 ohm in the dark to 387 ohm after irradiation. This large decrease in resistance is due to a large increase in the number of photoconductive carriers in the P3HT : PCBM induced by light irradiation. From this result, this semicircle recognized as photoactive layer.

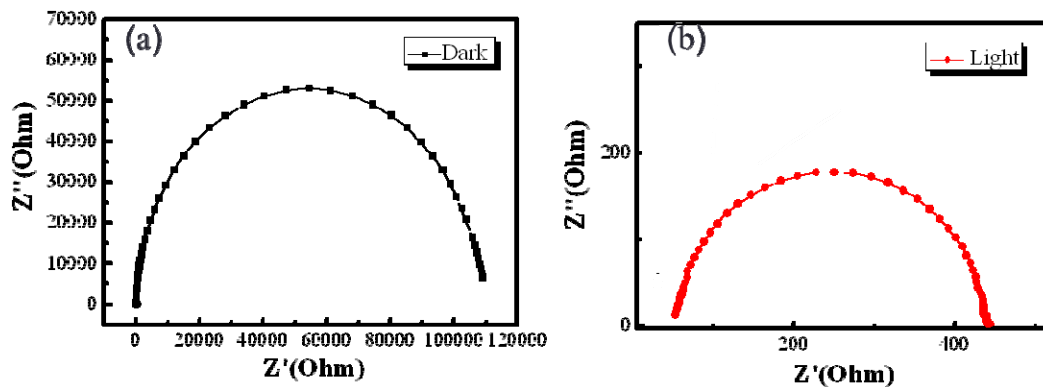


Fig. 4-20 The nyquist plots of device (a)dark 、(b)light

We observe the resistivity in active layer, measure the data under illumination for 2 hours. Fig. 4.20, the R_p value of the device without TiO_x increase with the irradiation time while TiO_x almost remain constant. The insert shows the equivalent circuit, the two equivalent is not the same, because of by introducing the titanium oxide into the device a p-n junction form between active layer and TiO_x , compare with the device without TiO_x , the CPE2 and R_2 added. The R_p value vs. irradiation time is depicted in Fig. 4.21. At 0 minute, the R_p value is 387, after illumination for 2hrs , the R_p value raise to 620.82. On the other hand, the R_p value of the device with TiO_x increase slightly with irradiation time. At 0 minute, the R_p value for the device with TiO_x is 155.87 and increase to 190 slightly for 2 hours under illumination.

The dramatically raised in R_p of device without TiO_x may due to the intrusion of oxygen and humidity into the photoactive layer and degrade the polymer. However, the TiO_x as a shield layer, effective protection of the polymer. Under illumination for long time, the devices still keep the high performance.

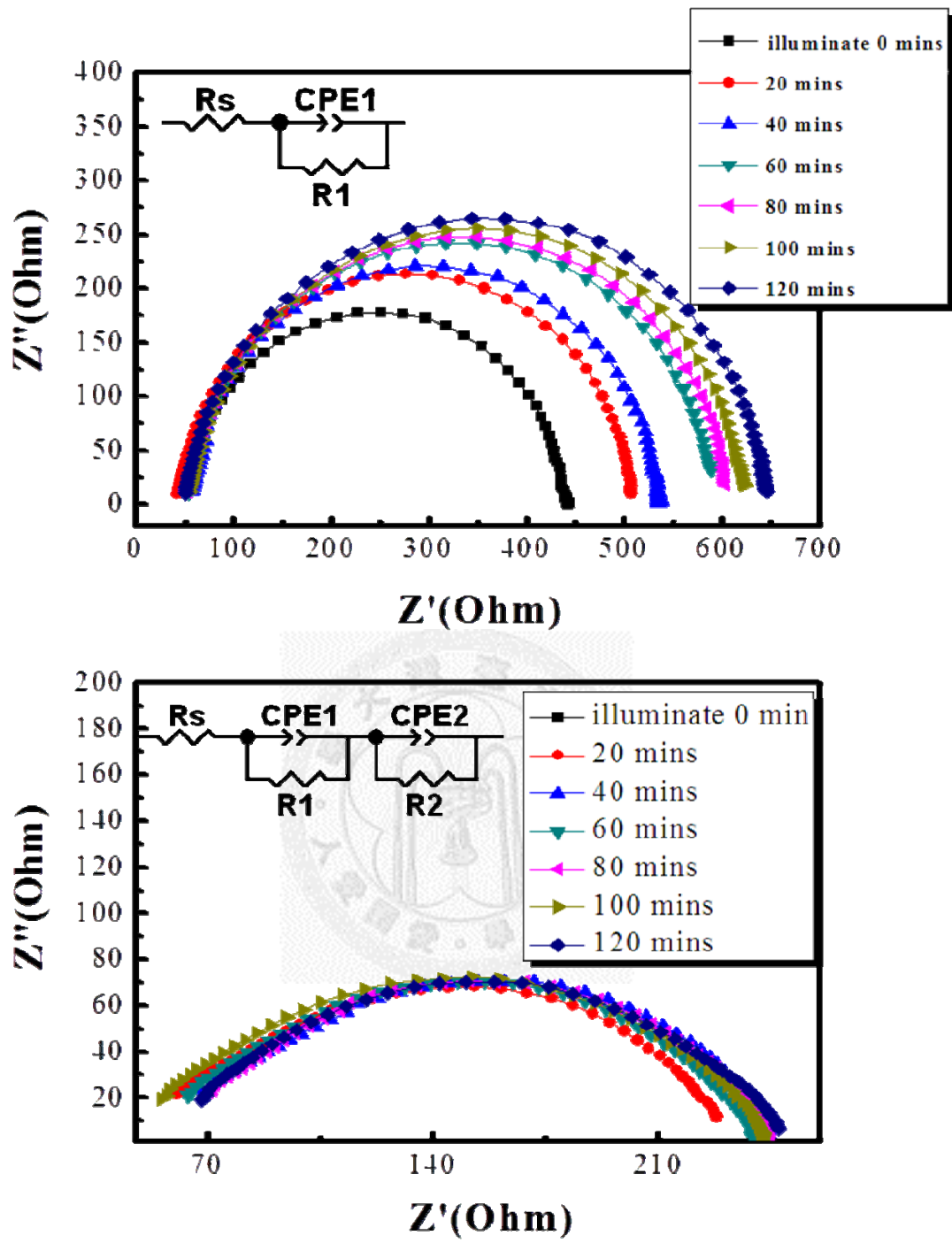


Fig. 4-21 The nyquist plots of device (a) without_x (b) with TiO_x

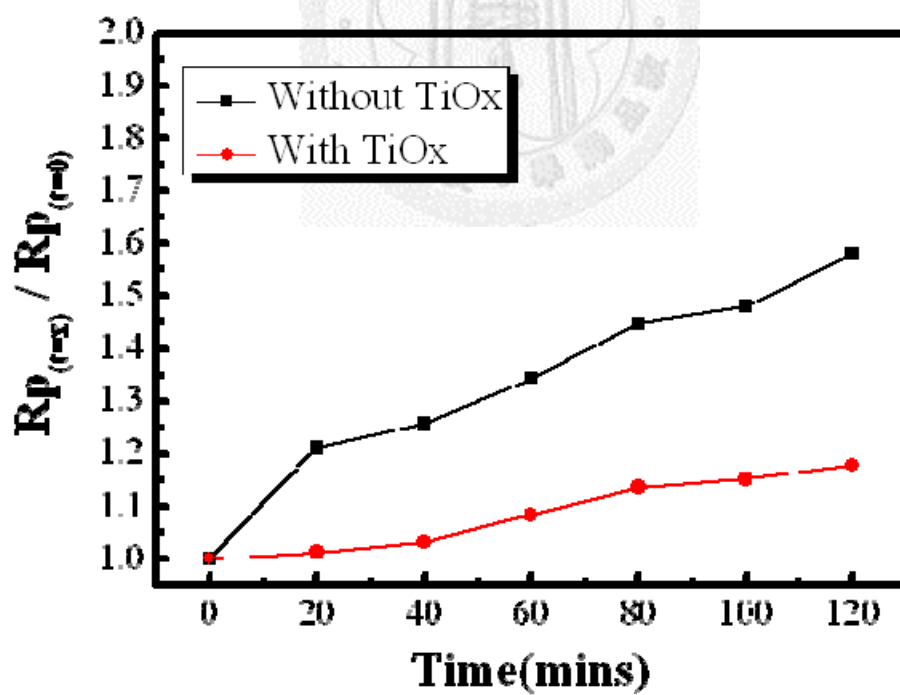
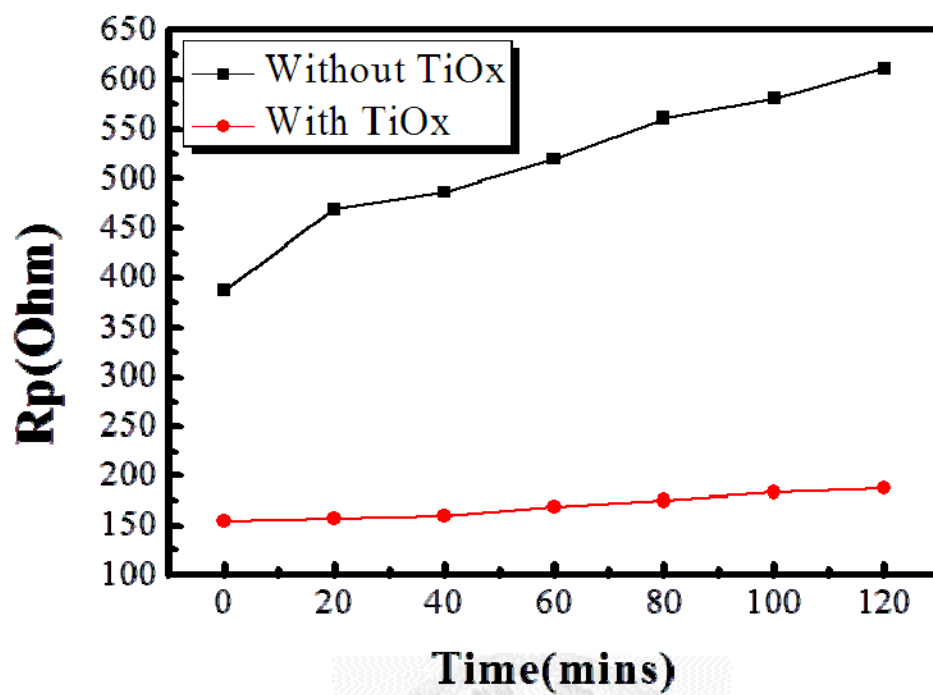


Fig. 4-22 The R_p value of device as a function of irradiation time.

4.5 Summary

Different O/Ti atomic ratio will effect the characteristics of titanium oxide, the conductivity and the conduction band level of TiO_x is related to the performance, therefore different device performance we observed.

By introducing TiO_x in OPV, it serves as protective layer for device and avoid the photoactive to deterioration effectively. In ambient air, the performance of device without TiO_x decay quickly, however the device with TiO_x still keep high performance for long time storage. Under illumination, the value of R_p for device without TiO_x increase almost double than initial value while the device with TiO_x increase slightly for 2 hours.



4.6 Reference

- [1] Kim, J. Y.; Kim, S. H.; Lee, H. H.; Lee, K.; Ma, W.; Gong, X.; Heeger, A. J., New Architecture for High-Efficiency Polymer Photovoltaic Cells Using Solution-Based Titanium Oxide as an Optical Spacer. *Advanced Materials* **2006**, *18* (5), 572-576.
- [2] Radecka, M.; Zakrzewska, K.; Czternastek, H.; Stapiński, T.; Debrus, S., The influence of thermal annealing on the structural, electrical and optical properties of TiO₂-x thin films. *Applied Surface Science* **1993**, *65–66* (0), 227-234.
- [3] Lin Yun-Yue “Solution Processible Polymer/Inorganic Nanomaterials Hybrid Solar Cells” National Taiwan University, Dissertation for Doctor of Philosophy
- [4] Xing, K. Z.; Johansson, N.; Beamson, G.; Clark, D. T.; Brédas, J.-L.; Salaneck, W. R., Photo-oxidation of poly(p-phenylenevinylene). *Advanced Materials* **1997**, *9* (13), 1027-1031.
- [5] Monkman, A. P.; Burrows, H. D.; da G. Miguel, M.; Hamblett, I.; Navaratnam, S., Measurement of the S₀–T₁ energy gap in poly(2-methoxy,5-(2'-ethyl-hexoxy)–p-phenylenevinylene) by triplet–triplet energy transfer. *Chemical Physics Letters* **1999**, *307* (5–6), 303-309.
- [6] Butterworth, M. D.; Corradi, R.; Johal, J.; Lascelles, S. F.; Maeda, S.; Armes, S. P., Zeta Potential Measurements on Conducting Polymer-Inorganic Oxide Nanocomposite Particles. *Journal of Colloid and Interface Science* **1995**, *174* (2), 510-517.
- [7] Park, M.-H.; Li, J.-H.; Kumar, A.; Li, G.; Yang, Y., Doping of the Metal Oxide Nanostructure and its Influence in Organic Electronics. *Advanced Functional Materials* **2009**, *19* (8), 1241-1246

- [8] C. J. Brabec, A. Cravino, D. Meissner, N. S. Sariciftci, T. Fromherz, M. T. Rispens, L. Sanchez, and J. C. Hummelen, *Advanced Functional Materials* **11** (5), 374 (2001).
- [9] V. D. Mihailetschi, P. W. M. Blom, J. C. Hummelen, and M. T. Rispens, *Journal of Applied Physics* **94** (10), 6849 (2003).



Chapter 5 Conclusions

In this research, we modify the O/Ti ratio of titanium oxide by an easy method, that is, controlled the reaction time. The O/Ti atomic ratio increase with reaction time and that will change the characteristics of the titanium oxide. Different O/Ti ratio cause different band gap, conduction band level and resistivity. By introducing titanium oxide layer between the active layer and the aluminum cathode in organic solar cell, the O/Ti ratio will effect the device performance. The titanium oxide with low O/Ti atomic ratio, it is the best one for electron transport layer in OPV because of its conduction level close to the LUMO of electron acceptor(PCBM) and the resistivity is also lower.

Air stability is a serious problems for the development of OPVs. The performance of conventional device(no external packaging or encapsulation were used) degraded in the air dramatically. However, by introducing TiO_x as a shielding layer, the device will remain high performance even storage in air for a long time.

In a nutshell, the TiO_x is not only a good electron transport layer that enhance efficiency but also provide a protection for photoactive layer, thereby, TiO_x improve the device performance and protect the photoactive layer effectively. It's foreseeable that the disadvantage of OPV can be can be overcome step by step.